

1 The “Missing Glaciations” of the Middle Pleistocene

2

3 **Philip D. Hughes¹, Philip L. Gibbard², Jürgen Ehlers³**4 ¹ Department of Geography, School of Environment, Education and Development,
5 The University of Manchester, Oxford Road, Manchester M13 9PL, United Kingdom6 ² Scott Polar Research Institute, University of Cambridge, Lensfield Road, Cambridge
7 CB2 1ER, United Kingdom8 ³ Hellberg 2a, D-21514 Witzeeze, Germany

9

10 **Abstract**

11 Global glaciations have varied in size and magnitude since the Early-Middle
12 Pleistocene transition (~773 ka), despite the apparent regular and high-amplitude 100
13 kyr pacing of glacial-interglacial cycles recorded in marine isotopic records. The
14 evidence on land indicates that patterns of glaciation varied dramatically between
15 different glacial-interglacial cycles. For example, MIS (Marine Isotope Stages) 8, 10
16 and 14 are all noticeably absent from many terrestrial glacial records in North
17 America and Europe. However, globally, the patterns are more complicated with
18 major glaciations recorded in MIS 8 in Asia and in parts of the Southern Hemisphere,
19 such as Patagonia for example. This spatial variability in glaciation between glacial-
20 interglacial cycles is likely to be driven by ice volume changes in the West Antarctic
21 Ice Sheet and associated interhemispheric connections through ocean-atmosphere
22 circulatory changes. The weak global glacial imprint in some glacial-interglacial
23 cycles is related to the pattern of global ice build-up. This is caused by feedback
24 mechanisms within glacier systems themselves which partly result from long-term
25 orbital changes driven by eccentricity.

26

27 **1. Introduction**

28 The most extensive and sustained glaciations in the Quaternary began in the last 900
29 kyr (*c.* MIS 24-22 to present) in the Northern Hemisphere and are associated with 100
30 kyr eccentricity-driven glacial-interglacial cycles (Head and Gibbard 2015; Hughes
31 and Gibbard 2018). Despite the obliquity-driven shorter 41 kyr glacial-interglacial
32 cycles of the earlier Pleistocene, there is evidence that high- and mid-latitudinal ice
33 sheets in the North Atlantic region have been present since the beginning of the

34 Pleistocene (Thierens et al. 2012). Southern Hemispheric glaciation is an even longer-
35 established phenomenon with substantial glaciation already a regular occurrence in
36 the Tertiary (Ehlers et al. 2018).

37

38 In the Italian Dolomites, glaciation became established in MIS 22 (Muttoni et al.
39 2003). Comparable evidence is also found north of the Alps in Switzerland and
40 southern Germany (Fiebig et al., 2011). However, the "Deckenschotter" glaciofluvial
41 deposits in Switzerland may represent earlier glaciation, and the older "Höhere
42 Deckenschotter" include vertebrate remains which suggest an age of 2.6-1.8 Ma
43 (Bolliger et al. 1996). The "Höhere Deckenschotter" are regarded as glaciofluvial
44 deposits. However, no till has been found as yet. In contrast, the "Tiefere
45 Deckenschotter" contain tills. Glaciation then might have been more extensive than in
46 the Würmian – see Figure 1 for global chronostratigraphical correlations. The age is
47 uncertain, but the deposits clearly predate the Middle Pleistocene (Preusser et al.
48 2011) when Schlüchter (1989) identified a major phase of geomorphological change
49 ("Mittelpleistozäne Wende") in the the Alps. The oldest glaciation identified in the
50 Pyrenees is of late Cromerian age (MIS 16 or 14) (Calvet, 2004). In North America,
51 widespread lowland glaciation (beyond Alaska and the Northern Territories) is first
52 seen during MIS 22 or 20 (Barendregt and Duk-Rodkin, 2011; Duk-Rodkin and
53 Barendregt, 2011). In South America, the extensive Great Patagonian Glaciation is
54 dated to 1.1 Ma and correlated with MIS 30-34 (Singer et al. 2004).

55

56 Following the Early Pleistocene precursors, glaciers reached lowland northern Europe
57 and Siberia in the early Middle Pleistocene shortly before the Brunhes–Matuyama
58 palaeomagnetic reversal (773 ka), which represents the boundary between the Early
59 and Middle Pleistocene (Head et al. 2008). These events laid down extensive sheets of
60 glaciogenic deposits across wide areas both on land and beneath the sea. In the
61 northern North Sea the formation of the Norwegian Channel caused an abrupt change
62 of sedimentary conditions at about this time (Ottesen et al. 2014). Whilst 100 kyr
63 cycles began c. MIS 24-22 (Elderfield et al. 2012), the largest amplitude 100 kyr
64 glaciations started with MIS 16, which marked the completion of the Early-Middle-
65 Pleistocene transition (Head and Gibbard 2005; Mudelsee and Schulz, 1997; Hughes
66 and Gibbard 2018).

67

68 Subsequently, major ice sheets repeatedly extended over large regions of North
69 America during the Middle Pleistocene pre-Illinoian events MIS 16, 12, 8 and 6
70 (Illinoian s.s.) and the Late Pleistocene MIS 4–2 (Wisconsinan). The Laurentide Ice
71 Sheet formed over large areas of Canada, reaching as far south as 38°N in the United
72 States during the Late Pleistocene (Dyke and Prest 1987) (Figure 2). More
73 significantly, the change in ice volume between glacial-interglacial cycles was the
74 largest single contribution to the global sea level changes. This was 70-90 m for the
75 last glacial-interglacial cycle (Stokes et al. 2012), which represents well over half of
76 the global ice contribution to glacial-interglacial sea level change. Today, the largest
77 ice sheet is restricted to Greenland with much smaller ice caps present in Canada.

78

79 The marine oxygen isotope record provides the main basis for defining Quaternary
80 glacial-interglacial cycles (Lisiecki and Raymo 2005) and has long been considered to
81 represent a record of global ice volume (Shackleton 1967). The marine isotope record
82 is widely used as the global reference with which the Quaternary can be subdivided
83 and the scheme of stages and substages in marine isotope record continues to
84 underpin the Quaternary timescale (Lisiecki and Raymo 2005; Railsback et al. 2015)
85 (Figure 1). The marine isotope record has the advantage of being derived from quasi-
86 continuous sedimentary sequences on the deep-ocean floors, whereas the glacier
87 records on land are inherently fragmentary. However, the marine isotope record is a
88 composite signal of fluctuations in global ice volume and does not provide
89 information on the spatial pattern of glaciations. Furthermore, since changes in global
90 ice volume are dominated by the Laurentide Ice Sheet (Figure 2) it is not necessarily
91 representative of the pattern and scale of glaciations in other parts of the world. This
92 poses problems for direct terrestrial-marine correlation (Gibbard and West 2000) and
93 care must be taken to isolate glacier records using single proxies such as the marine
94 isotope record. This is also true for other indirect proxies for global glaciations, some
95 of which are utilized here such as sea level and ice core records. Thus, a collective
96 approach is necessary to decipher the patterns of global glaciations, especially where
97 terrestrial glacial records are absent, ambiguous or poorly dated, which is often the
98 case especially for the Middle Pleistocene glaciations.

99

100 The application of numerical dating of Late Pleistocene glaciations is increasingly
101 demonstrating the asynchronies in the timing of glacial maxima on a global scale
102 (Hughes et al. 2013). Whilst the differing timing of mountain glaciations compared to
103 the continental ice sheets has been known for decades (e.g. Gillespie and Molnar
104 1995), there is now also evidence that the timing of maximum extents of major ice
105 sheet margins may have differed by as much as tens of thousands of years. Such
106 differences appear to result from the contrasting regional geographical situation,
107 where differing ocean and atmospheric circulatory patterns influence the precipitation
108 and air temperatures (Hughes et al. 2013).

109

110 Differences in the pattern and timing of glacial extent are also notable between
111 different glacial-interglacial cycles (cf. Margari et al. 2010; 2014; Hughes and
112 Gibbard 2018; Batchelor et al. 2019). The largest glaciations of the last 800 kyr, such
113 as in MIS 5d-2, were characterised by an early advance of glaciers followed by an
114 interlude then a second major advance leading to the global glacial maxima within the
115 glacial-interglacial cycles (Hughes and Gibbard 2018). This corresponds to the classic
116 asymmetrical pattern of ice build-up in 100 kyr glacial-interglacial cycles (Broecker
117 and van Donk 1970). The greater magnitude of the second major global ice advance is
118 reflected in the larger dust peak associated with this compared to the first major
119 advance, such as when comparing MIS 4 and 2 in the last glacial-interglacial cycle
120 (Figure 3). However, Hughes and Gibbard (2018) identified differences between
121 glacial-interglacial cycles with some exhibiting different patterns. For example, in
122 MIS 10 and 8 the first phase of glacier build-up corresponded to the largest dust peaks
123 and the later global glacial maxima was associated with much smaller dust peaks in
124 Antarctic ice-core records (Figure 4). Other anomalies are also evident when
125 considering the pattern of glaciations from the perspective of the marine isotope
126 record. For example, some major stadials occur within interglacial complexes (such as
127 MIS 7d) (Ruddiman and McIntyre 1982). These represent “missing glaciations” in the
128 sense that they are rarely recorded on land. However, it is important to understand
129 that glaciers would have been more extensive than today in most areas of the world in
130 all cold intervals of major glacial-interglacial cycles. The evidence that glaciations are
131 “missing” simply arises because their spatial coverage has been overridden by later
132 more extensive glaciations.

133

134 We test the hypothesis that the cold phases of some glacial-interglacial cycles were
135 characterised by less extensive glaciations than others. In order to do this, this article
136 examines the evidence for Middle Pleistocene glaciations after MIS 16, which marked
137 the onset of the largest 100 ka glacial cycles (Hughes and Gibbard 2018). We focus
138 on MIS 8, 10 and 14 together with other intermediate intervals (MIS 7d, MIS 13b and
139 15b) and test whether the concept of “missing glaciations” is valid for these cold
140 intervals. We aim to explore reasons for the differences in the terrestrial glacial
141 records between and within glacial-interglacial cycles by examining both the wider
142 environmental imprint of global glaciations alongside the drivers of global climate
143 change.

144

145 **2. Methodological Approach**

146

147 **2.1. Glacial records**

148 The geological and geomorphological evidence for glaciation is based on numerous
149 published papers from sites around the world. This evidence includes large
150 compilations and reviews such as those in Ehlers et al. (2011a, b) and many other
151 sources, including many new datasets from the last few years. A key focus is on dated
152 records, which for the Middle Pleistocene glacial record are dominated by
153 cosmogenic exposure, optically stimulated luminescence, and uranium-series dating.

154

155

156 **2.2. Indirect records of glaciation and global climate**

157

158 **2.2.1. Marine isotope records**

159 Marine oxygen isotope records provide the classic proxy for global ice volume
160 (Shackleton 1967) and underpin modelling approaches for ice sheet reconstructions
161 through time where direct evidence of glaciation is not available (e.g. Batchelor et al.
162 2019). The driver of cyclic fluctuations in marine oxygen isotopes from foraminiferan
163 tests has long been attributed to orbital forcing (Hays et al. 1976) and this provides
164 the timeframe to which the marine isotope record is tuned (Imbrie et al. 1984,
165 Ruddiman et al. 1989; Lisiecki and Raymo 2005) (Figure 4). However, the marine
166 oxygen isotope record is not a pure record of global ice volume but is a record of both
167 global ice volume and deep ocean temperature (Spratt and Lisiecki 2016).

168 Furthermore, as noted earlier, changes in the Laurentide Ice Sheet through glacial-
169 interglacial cycles dominate the global ice volume component of the marine isotopic
170 signal due to its large size relative to other ice masses on Earth (Figure 2).
171 Consequently, the marine isotope record is not representative of the spatial
172 complexity of global glaciations (Hughes et al. 2013).

173

174 2.2.2. Sea-level records

175 Global ice volume is closely intertwined with global sea levels and the magnitude of
176 glaciations is reflected in sea-level changes. Global sea levels through the last 800 kyr
177 were assessed using the data of Spratt & Lisiecki (2016) (Figure 4). In their paper,
178 Spratt and Lisiecki (2016) analysed seven Late Pleistocene sea-level records for the
179 interval 0-430 kyr and five for the interval 0-798 kyr that have converted the oxygen
180 isotope content of the calcite tests of foraminifera ($\delta^{18}\text{O}_c$) to sea level. The seven
181 records included an inverse ice volume model (Bintanja et al., 2005), Pacific benthic
182 $\delta^{18}\text{O}$ of seawater ($\delta^{18}\text{O}_{sw}$) (Elderfield et al., 2012), a global stack of planktonic $\delta^{18}\text{O}_{sw}$
183 (Shakun et al., 2015), Relative Sea Level from the Mediterranean (Rohling et al.,
184 2014), Atlantic benthic $\delta^{18}\text{O}_{sw}$ (Sosdian and Rosenthal, 2009), $\delta^{18}\text{O}_c$ regression
185 (Waelbroeck et al., 2002) and a Relative Sea Level from the Red Sea (Rohling et al.,
186 2009). The longer record (used in this paper) for interval 0-798 kyr excluded the $\delta^{18}\text{O}_c$
187 regression (Waelbroeck et al., 2002) and the Relative Sea Level from the Red Sea
188 (Rohling et al., 2009) (see Spratt and Lisiecki 2016, their Table 1).

189

190 Hughes and Gibbard (2018) analysed sea-level changes through glacial-interglacial
191 cycles using the data of Shakun et al. (2015), who used planktonic $\delta^{18}\text{O}_{sw}$ to correct
192 the $\delta^{18}\text{O}$ stack for non-ice volume effects. However, in their analysis of global sea-
193 level change through glacial-interglacial cycles, Spratt and Lisiecki (2016) noted that
194 because the surface ocean is affected by greater hydrological variability and
195 characterises a smaller ocean volume than the deep ocean, then planktonic $\delta^{18}\text{O}_{sw}$
196 may differ more from ice volume changes than benthic data.

197

198 2.2.3. Sea-surface temperature records

199 Shakun et al. (2015) exploited the temperature component of planktonic $\delta^{18}\text{O}$ records
200 from 49 cores around the globe to calculate a stacked record of global sea surface
201 temperatures (Figure 4). This now enables insights into global shifts in both climate

202 and ice volume during glacial-interglacial cycles. This is significant because it avoids
203 the Laurentide problem, where global ice volumes are dominated by a single regional
204 ice mass. Whilst ice sheets do affect sea-surface temperatures at the regional scale,
205 global sea-surface temperatures between different oceans are much less likely to be
206 dominated by regional ice dynamics.

207

208 Whilst the surface ocean is undoubtedly subject to greater hydrological variability (cf.
209 Spratt and Lisiecki 2015) and surface atmospheric processes, this is useful for
210 gauging the state of the Earth's ocean-atmosphere interface. At individual scales, sea-
211 surface temperature records are likely to be quite variable, but when combined the
212 stack of 49 cores utilized by Shakun et al. (2015) from sites located at 0-60 N and S in
213 the Pacific, Atlantic and Indian Oceans does provide a global summary of the state of
214 the ocean-atmosphere interface through glacial-interglacial cycles.

215

216 2.2.4. Ice-core records

217 Dust content in polar ice cores can provide insights into the state of the global
218 atmosphere through time and this was utilized by Lambert et al. (2008; 2012) to
219 assess dust flux over Antarctica during multiple glacial-interglacial cycles. Hughes
220 and Gibbard (2018) argued that peaks in Antarctic dust in glacial-interglacial cycles
221 corresponded to global ice build-up in both hemispheres and this was used as an
222 indirect indicator of global glacial behaviour in glacial-interglacial cycles. This
223 argument was largely built on the observations from the last glacial-interglacial cycle
224 where large ice build-up in MIS 4 and 2, for example, was associated with peaks in
225 dust not only in Greenland but also in Antarctica (Hughes et al. 2013) (Figure 3).

226

227 Given that the Greenland ice-core records only span from the last Interglacial,
228 Antarctic records must be relied upon for earlier glacial-interglacial cycles. Dust flux
229 over Antarctica has a close correlation with temperature as climate becomes colder
230 (Lambert et al. 2008). Comparison of Antarctic ice-core dust records with
231 loess/palaeosol sequences from the Chinese Loess Plateau (Kukla et al. 1994)
232 confirms the synchronicity of global changes in atmospheric dust load (Lambert et al.
233 2008). However, being a Southern Hemisphere record, comparisons of dust peak
234 magnitudes cannot necessarily be transferred to interpreting the size of global ice
235 volume, only the temporal pattern and possibly the hemispheric distribution of ice

236 masses. Nevertheless, Antarctic dust records are broadly representative of the global
237 hydrological cycle with increasing dust indicating a cooler and drier global
238 atmosphere that is directly associated with the extent of global glaciations.

239

240 Dust records may be a better reflection of global ice spatial coverage on land than
241 marine isotope records, which partially reflect ice volume. This is because increased
242 ice coverage over land surfaces causes increased aridity in peripheral areas due to the
243 effects of ice masses on regional climate (Manabe and Broccoli 1985). This occurs
244 today where strong anticyclones form over modern ice sheets (Hobbs 1945). The
245 aridity effects would have been compounded during the Pleistocene cold phases due
246 to effects of not just low precipitation but also low atmospheric CO₂ on plant
247 growth (Claquin et al. 2003).

248

249 **2.3. Drivers of global glaciations - Solar forcing and CO₂**

250 We examine the patterns of Earth-orbital changes and glacial-interglacial cycles to see
251 if there is any relationship between “missing glaciations” and orbital forcing. Solar
252 radiation is important when considering glaciations because it controls the energy
253 receipt to the Earth and thereby impacts on glacier mass balance, especially ablation.

254 In their synthesis of the last ten glacial-interglacial cycles, Hughes and Gibbard
255 (2018) showed that variations in solar radiation in the Northern Hemisphere was
256 responsible for ~50-60% of variations in global ice volume. For example, troughs in
257 solar radiation at the end of interglacials and beginning of subsequent cold stages are
258 thought to be associated with rapid glacier advances in the continental interiors and
259 high- and mid-latitude mountains (Hughes and Gibbard 2018). This hypothesis is
260 tested further here by quantifying the magnitude of solar peak-trough changes at the
261 transition between interglacial and glacial intervals (Figure 4). This was done by
262 calculating a value for **solar-trough magnitude (STM)**, which describes the trough
263 magnitude and timespan at 60°N. This is derived by taking the median (50th
264 percentile) solar radiation value (W m⁻²) between the trough and the preceding peak
265 (s_m) and dividing this by the trough timespan (s_t) (defined by the time in years
266 between the trough and the preceding peak), then inverting this value:

267

$$268 \text{ STM} = 1/(s_m/s_t)$$

269

270 We also examine the orbital record further by isolating the effects of orbital
271 parameters such as eccentricity, obliquity and precession, on global glacier dynamics
272 within and between glacial-interglacial cycles. Eccentricity controls the shape of the
273 Earth's orbit around the sun and directly affects the influence of variations of
274 precession (i.e. on the timing of peri- and aphelion), and the seasonal distribution of
275 solar radiation. The interaction of eccentricity with precession is indicated in the
276 precession index (Figure 4). In addition to solar radiation, Ganopolski et al. (2016)
277 highlighted the importance of CO₂ in glacial inception. They identified points in time
278 where low CO₂ corresponded with low insolation as potential triggers for global ice
279 build-up. This hypothesis implies that low insolation alone cannot explain global
280 glacial inception. Instead, it is the combination of insolation forcing with atmospheric
281 CO₂ concentrations that drives glacial inceptions. Over the longer term, declining
282 atmospheric CO₂ through the Quaternary has been linked to the removal of weathered
283 regolith by glacial erosion over North America and Europe (Clark and Pollard 1998).
284 This causal mechanism may partly explain the transition to the large-magnitude 100
285 ka glacial-interglacial cycles at the Early-Middle-Pleistocene transition (Clark and
286 Pollard 1998; Ganopolski and Calov 2011; Tabor and Poulson 2016; Willeit et al.
287 2019).

288

289 **2.4 Terminology**

290 There are three ways to define glacial-interglacial cycles (Hughes and Gibbard 2018):

- 291 1) The periods between glacial terminations.
- 292 2) The periods of cold phases defined by global sea surface temperatures within
293 glacial-interglacial cycles (cf. Shakun et al. 2015), and;
- 294 3) The span of traditional subdivision of cold intervals based on Marine Isotope
295 Stages and substages (Railsback et al. 2015).

296

297 The term “cold stage” refers to climatostratigraphical/chronostratigraphical units such
298 as the Weichselian or Wisconsinan in Europe or North America, respectively, which
299 are equivalent to MIS 5d-2. This is complicated by the fact that some cold stages in
300 this definition span multiple glacial-interglacial cycles, such as the Saalian and
301 Wolstonian Stages in continental Europe and the British Isles, respectively. Marine
302 oxygen isotope stages are distinct from chronostratigraphical cold stages and

303 sometimes multiple Marine Isotope Stages make up a single cold stage in the strict
304 sense. For example, the Weichselian/Wisconsinan stages include MIS 5d-2 and also
305 the early part of MIS 1. A global correlation table based on the chart of Cohen and
306 Gibbard (2011) is provided in Figure 1 to aid cross-comparison between marine
307 isotope events and terrestrial chronostratigraphy.

308

309 **3. The “missing glaciations”**

310

311 **3.1. MIS 8 (Middle Saalian and equivalents)**

312 MIS 8 occurs within a larger glacial-interglacial cycle between termination IV and III
313 (Figure 4). Overall, this was a relatively weak glacial-interglacial cycle. The glacial
314 inception occurred at the boundary of MIS 9d/e at c. 320 ka. MIS 8 has a weak signal
315 of global glaciation in many records, particularly benthic $\delta^{18}\text{O}$ (Lang and Wolff 2011)
316 and second only to MIS 14 in terms of maximum $\delta^{18}\text{O}$ values for the last ten glacial-
317 interglacial cycles (Figure 4). At -93.27 m, MIS 8 had the highest sea levels of the last
318 six 100 kyr glaciations (Table 1). The lowest sea levels do not coincide with the
319 trough in benthic $\delta^{18}\text{O}$ values (at 252 ka) but occurred c. 18 kyr earlier at 270 ka in
320 MIS 8c (Figure 4). A strong interstadial (MIS 9a) separates two marine isotopic
321 troughs (MIS 8a-c and 9b).

322

323 The solar-trough magnitude at the beginning of this glacial-interglacial cycle was one
324 of the weakest of the seven glacial-interglacial cycles (Table 2). This is likely to have
325 resulted in a weak glacial inception and explains the weak stadial conditions in MIS
326 9d, which is characterised by relatively minor excursions in benthic and planktonic
327 isotope values and moderate influence of sub-polar water masses (Roucoux et al.
328 2006). In their core from the Iberian margin, Roucoux et al. (2006) argued that the
329 pollen evidence suggests a less arid and cold climate than during other stadial
330 intervals where steppe was more abundant, and temperatures offshore were lower.

331

332 Dust flux over Antarctica for MIS 8 reached some of the highest and sustained levels
333 of the last million years, reaching values comparable with MIS 6, yet more sustained,
334 and greater than MIS 5d-2 (Figure 4). Significantly, the dust peak in Antarctica does
335 not coincide with the largest marine isotope trough of MIS 8a. Instead, it occurs
336 earlier at c. 272 ka in MIS 8c, coinciding with the lowest sea levels. Hughes and

337 Gibbard (2018) noted that the first dust peak also coincides with the lowest CO₂
338 levels (Ganopolski et al. 2016) and the coldest global sea surface temperatures of this
339 glacial period (Shakun et al. 2015). Pollen records from a marine core on the Iberian
340 margin match these patterns and show the most extreme glacial conditions of MIS 8
341 occurred during the early part, followed by an interval of warmer conditions and tree
342 population expansion after 263 ka (Roucoux et al. 2006). This suggests that the
343 configuration of controls of global climate (including insolation, atmospheric
344 composition, land cover, sea ice and the ice sheets themselves) were different in MIS
345 8 from other glaciations, such as MIS 6 and 5d-2. In these later glaciations, the global
346 ice maxima and associated cold and dry indicators occurred towards the end of the
347 glacial-interglacial cycle.

348

349 Examination of the record of glaciation during this period (i.e. c. 300-245 ka)
350 repeatedly shows that evidence of glaciation is poorly represented throughout much of
351 the world's glaciated regions. In northern Europe the traces of glaciation that can be
352 reliably attributed to this time are rare. The few deposits that have been identified in
353 North-West Europe are mainly based on isolated numerical age determinations,
354 especially optically stimulated luminescence (OSL) or amino-acid racemisation
355 analyses of adjacent sediments or their contained fossil materials. For example, the
356 most often quoted example is that reported by Beets et al. (2005) suggesting that pre-
357 Late Saalian (i.e. Middle Saalian; MIS 8) till occurs in the North Sea basin based on
358 geophysical, micropalaeontological and amino-acid age evidence. Whilst there is no
359 question that till occurs at the site, there remains scepticism about the age attribution
360 among Dutch workers who generally attribute these deposits to the Late Saalian (MIS
361 6; Cohen 2017, personal communication). Despite other possible MIS 8 records from
362 other circum-North Sea localities (e.g. Davies et al. 2012; White et al. 2010; 2017;
363 Bridgland et al. 2014; Roskosch et al. 2015) all of these remain equally equivocal. In
364 contrast, as in the Netherlands, recent dating evidence from eastern England has
365 confirmed that a major glaciation did occur in MIS 6 (Evans et al. 2019) confirming
366 the Wolstonian (=Saalian) age of a glaciation that reached into the Fenland basin in
367 eastern England (Gibbard et al. 2018). The lack of a regional till sheet and consistent
368 biostratigraphy appears to support the view that glacial ice did not extend into the
369 central western European area and the central and southern North Sea basin (Huuse
370 2017, personal communication) during MIS 8. However, there is evidence for Middle

371 Saalian glaciation that reached the continental shelf edge off-Norway, Svalbard and
372 Scotland, according to Sejrup et al. (2000; 2005). In southern Jæren this glaciation is
373 represented by the Vigrestad Till (glacial F: Sejrup et al. 2000). In Denmark
374 westward flowing meltwater streams deposited sand and gravels over much of central
375 and southern Jylland. These streams derive from the first Saalian ice advance that
376 occurred during MIS 8, which deposited the Treldenæs Till (Houmark-Nielsen, 2004,
377 2011). This Norwegian Saale Advance invaded Denmark from the north, probably
378 terminating south of the Danish-German border in Schleswig-Holstein (Houmark-
379 Nielsen 2011).

380

381 In North-West Europe, Toucanne et al. (2009a) noted that ‘Fleuve Manche’ fluvial
382 discharge through the English Channel was significantly less during MIS 8 than
383 during MIS 6 and MIS 2 (indicated by lower mass accumulation rates (MAR) in
384 Figure 6). This is consistent with smaller ice masses in northern Europe and the Alps,
385 the meltwater from which drained into this river system in MIS 8. Furthermore, in the
386 Northeast Atlantic Ocean at ODP 980 (55°29’N, 14°42’W) summer sea-surface
387 temperatures were generally warmer in MIS 8 than in MIS 6 and 2 (McManus et al.
388 1999). However, oscillations in SSTs were large with minimum temperatures on a
389 par with MIS 6 and 2. In fact, the quantities of ice rafted debris in the NE Atlantic
390 during MIS 8 and 10 were significantly larger than in MIS 6 and 2 (McManus et al.
391 1999). This was related to high-amplitude millennial scale climate change, which is
392 also reflected in terrestrial vegetation records in Europe (Fletcher et al. 2013). The
393 muted signal in the ‘Fleuve Manche’ discharge in contrast to a strong signal in the
394 ice-rafted debris (IRD) in the NE Atlantic suggests the configuration of ice masses in
395 this region differed between glacial-interglacial cycles.

396

397 In Poland, the Krznanian glaciations are correlated with MIS 8 (Lindner and Marks
398 1999). According to Marks (2011) Poland was invaded by ice sheets derived from
399 Scandinavia during the Liwiecian, Krznanian and Odranian intervals within the
400 Saalian Stage. The limit of the Odranian glaciation can be mapped at the modern land
401 surface, whereas the Liwiecian and Krznanian are buried by younger deposits.
402 During the latter an ice sheet advanced into eastern Poland, reaching as far south as
403 the northern foreland of the South Polish Uplands, and it probably also approached

404 the Silesian Upland. This advance may have also crossed the Baltic States, Latvia
405 and Lithuania and presumably parts of Belarus.

406

407 In neighbouring European Russia, glaciation during this period seems to have been
408 markedly less extensive than during the Late Saalian-equivalent Dniepr and Moscow
409 glaciations (MIS 6) (Velichko et al. 2011) (Figure 1). However, east of the Urals it is
410 represented by the substantial till of the Samarovo glaciation, the deposits of which
411 form the maximum glacial drift boundary in western Siberia. This major glaciation is
412 correlated with MIS 8 (Figure 5) based on regional stratigraphical successions
413 (Astakhov et al. 2016).

414

415 Whilst the limit is based on boreholes and rare natural sections in the West Siberian
416 Plain, in the Central Siberian uplands the boundary has been mapped based on chains
417 of push moraines and occasionally where it overlies interglacial fluvial deposits in
418 buried valleys (Rudenko et al., 1984; Astakhov 2011). In the Western Siberian Plain
419 and the Central Siberian Plateau the Samarovo glaciation was consistently much more
420 extensive than the later Taz glaciation which is thought to date from later in the
421 Saalian Stage in MIS 6 (Astakhov et al 2016). Given the scale of the land areas
422 involved these Siberian ice masses would have been major contributors to global ice
423 volume.

424

425 In the mountains of central and southern Europe, evidence of glaciation in MIS 8 has
426 been recognised in Iberia (Fernández Mosquera et al. 2000; Vidal Romaní *et al.*
427 2015), Italy (Giraudi and Giaccio 2017) and in the Alps (Preusser et al. 2011). In
428 Baden-Württemberg and Bavaria the multi-phased Riss Glaciation is provisionally
429 correlated with MIS 10-6 (Doppler et al. 2011). In the Balkans there is also some
430 evidence of MIS 8 glaciation (Hughes et al. 2011). In the Italian Apennines, Giraudi
431 et al. (2011) reported that there was no evidence for glaciation in MIS 8, unlike for
432 other Middle Pleistocene glaciations. However, later work in the same basin revealed
433 evidence of two glaciations between 350 and 130 kyr and these were correlated with
434 MIS 8 and 6, although the relative sizes of these two glaciations was not established
435 (Giraudi and Giaccio 2017).

436

437 In North America evidence of glaciation attributed to the MIS 8 interval is equally
438 elusive. In North-West Canada and eastern Alaska where till and associated deposits
439 of the Reid Glaciation are frequent (Duk-Rodkin et al. 2004; Duk-Rodkin and
440 Barendregt 2011), there is some doubt regarding the correlation of these materials to
441 either MIS 6 or 8, both, or in some cases younger intervals (Ward et al., 2008; cf.
442 Duk-Rodkin et al. 2004; Barendregt & Duk-Rodkin 2011 for discussion). In some
443 areas, OSL dating of glaciofluvial deposits over- and underlying till has determined
444 the age of the Reid Glaciation as MIS 6 (Demuro et al. 2012). Equivalents to the MIS
445 6 or 8 glaciations are almost certainly present in the Mackenzie Mountains, where as
446 many as three tills occur beneath the Late Pleistocene Laurentide glacial deposits at
447 the surface. On Banks Island in the Canadian Arctic, till underlying last interglacial
448 (Sangamonian Stage) Cape Collinson glaciomarine deposits are termed the Thomsen
449 Glaciation (250 ka). These deposits are thought to mark the maximum extent of
450 Middle Pleistocene glaciation in north-western Canada (Duk-Rodkin et al. 2004).
451

452 Elsewhere in North America evidence is found in the Sierra Nevada where several till
453 units appear to date from the MIS 8–6 (303–186 ka) interval, but here the age control
454 is insufficient to distinguish to which individual events they relate (Gillespie &
455 Zehfuss 2004; Gillespie and Clark 2011). Despite previous reports of MIS 8-age
456 glacial deposits in Glacier National Park, the early Bull Lake Till (Richmond 1986), it
457 is now thought that no deposits of this age occur in this district (Fullerton et al. 2004).
458 In Illinois, the southern margin of the Middle Pleistocene Laurentide Ice Sheet
459 extended 150 km beyond the later Wisconsinan (MIS 5d–2) limits. Stiff & Hansel
460 (2004) suggested that glacial deposits of MIS 8 may be present in these more
461 extensive limits. However, Curry et al. (2011) argue that the combination of evidence
462 from palaeosols and a range of different dating techniques (OSL, ^{10}Be , amino-acid
463 geochronology) indicate that the Illinoian glaciation is restricted to MIS 6. In
464 Missouri, till units have been shown to pre-date MIS 6 using ^{10}Be burial dating,
465 although the imprecision of this technique means that correlations for these tills can
466 be made with MIS 8, 10 or even 12 (Rovey and Balco 2011). In western Wisconsin
467 two till formations are related to the ‘Illinoian Glaciation’ (*s.l.*) which in the region is
468 dated to 300-130 ka (Syverson & Colgan 2004, 2011). These units, derived from the
469 Superior province, extend beyond the Wisconsinan ice-maximum limits. However it
470 is not known to which marine isotope stage they relate. Patchy deposits of similar age

471 occur in southern Wisconsin and northern Illinois (Syverson and Colgan 2004; 2011),
472 but again may relate to MIS 6.

473

474 In South America evidence from the tropics is once again rather limited, although
475 there is strong evidence of MIS 8 glaciation in Patagonia. Here, ^{10}Be concentrations in
476 outwash cobbles indicate a major glacial advance at c. 260 ka, within MIS 8. This is
477 coincident with the most pronounced dust peak in MIS 8 in Antarctic ice cores (Hein
478 et al. 2009). Significantly, Hein et al. (2009; 2017) found that exposure ages from
479 dated outwash terraces are 70-100 ka older than the associated moraines. Based on
480 geomorphological observations, they suggested that this difference can be explained
481 by exhumation of moraine boulders.

482

483 Elsewhere in the Southern Hemisphere, the large moraines occurring at the mouths of
484 valleys and cirque basins in western Tasmania were thought to have marked the Last
485 Glaciation (MIS 2) limits, such as in the West Coast Range (Lewis, 1945; Colhoun,
486 1985). However, recent exposure dating has demonstrated that this is incorrect and
487 that some of these moraines were formed during the Middle Pleistocene (Barrows et
488 al., 2002; Kiernan et al. 2010). In their review, Colhoun & Barrows (2011, p. 1042)
489 stated that the Hamilton Moraine, west of Lake Margaret, formed during MIS 8.

490

491 In New Zealand, weathered till, correlated with MIS 8 (Rattenbury et al., 2006), near
492 Edwards Pass between the Waiau and Clarence valleys, lies about 20 km down valley
493 from the MIS 2 termini. However, a geochronological basis for this correlation is
494 lacking and for most glaciations pre-dating MIS 6 correlations with the marine
495 isotope record are made using relative and biostratigraphical criteria (Barrell 2011).
496 With respect to the Middle Pleistocene glaciations in New Zealand, only MIS 6
497 glaciations have been confirmed by dating (e.g. Rother et al. 2010).

498

499 Overall, glaciation associated with MIS 8 is rarely found or at least not conclusively
500 confirmed in most regions. Glacier extents in MIS 6 were consistently larger and this
501 is supported by a much wider body of evidence. Major exceptions to this occur in
502 Russia east of the Urals and in Patagonia.

503

504 **3.2. MIS 10**

505 Superficially, the isotope sequence for MIS 10 resembles those of other major
506 glaciations, with a similar structure to MIS 12, but less severe. For example, global
507 sea-levels were -102.83 m compared with -124.4 for MIS 12, yet >9 m lower than in
508 MIS 8 (Table 1). However, the dust record from Antarctica indicates two major dust
509 peaks, one at c. 341-342 ka corresponding with the ‘glacial maximum’ indicated in
510 the marine isotope record (MIS 10a) and another even larger dust peak earlier in the
511 glacial-interglacial cycle at c. 355 ka (Figure 4). The largest dust peak occurs in
512 substage MIS 10b and corresponds with an early sea level trough of -92.82 at 356 ka.
513 This dust peak and low sea level stand is preceded by the coldest part of MIS 10 (at
514 the start of MIS 10c) recorded in global sea-surface temperatures (Figure 4; Shakun et
515 al. 2015) and the lowest atmospheric CO₂ levels of the glacial-interglacial cycle
516 (Hughes and Gibbard 2018).

517

518 Solar radiation in the Northern Hemisphere was lowest late in the glacial-interglacial
519 cycle, close in time to the glacial maximum indicated in the marine isotopic record
520 (Figure 4). Before this insolation was relatively high and sustained at >480 W m⁻²
521 with only minor troughs earlier in the glacial-interglacial cycle, except for a more
522 significant trough at the MIS 11c/11b boundary which marks the beginning of the
523 glacial-interglacial cycle. The solar-trough magnitude at the preceding
524 interglacial/glacial transition was weakest of all the last seven glacial-interglacial
525 cycles (Table 2).

526

527 Like MIS 8, glacial deposits dating from the interval represented by MIS 10 (c. 375-
528 340 ka) are very poorly represented in North-West Europe. In the southern and central
529 North Sea region there is no record, although Norwegian and Svalbard ice extended to
530 the shelf-margin as indicated in offshore accumulations, according to Sejrup et al.
531 (2005) and is confirmed by IRD. The glaciation is represented by an unnamed till,
532 underlying the Varhaug marine sediments in the Hobberstad borehole (Sejrup et al.
533 2000). In North Sea surveys Graham (2007) mapped ice-stream bed structures within
534 the Coal Pit Formation, in the Witch Ground basin. Although the age correlation in
535 this basin is not ideal, the features suggest shelf glaciation between MIS 10–6
536 (Graham et al. 2011). However, as in MIS 8 the ice was most probably markedly
537 more limited in extent. Scandinavian and British ice masses were almost certainly not
538 confluent across the North Sea basin during these phases (Toucanne et al., 2009a, b).

539 As with the MIS 8 evidence, there are some isolated age determinations that did hint
540 at possible MIS 10-age glacial advances, e.g. Scourse et al. (1999) in the Nar Valley
541 area of Norfolk in eastern England. However, these determinations have been
542 questioned and more recently rejected (Gibbard & Clark 2011). Whilst ice masses
543 over NW Europe were restricted in MIS 10, there was nevertheless significant ice-
544 rafting in the North Atlantic reaching as far south as the Bay of Biscay (e.g. McManus
545 et al. 1999; Toucanne et al. 2009a) (Figure 6).

546

547 Elsewhere in Europe the evidence for MIS 10-equivalent age glaciation is
548 fragmentary. In the Alps, glaciation may have happened, but the evidence has not
549 been dated (Van Husen & Reitner, 2011). Poland once again preserves a record of
550 post-Holsteinian (Mazovian) Interglacial Stage glaciation that has been correlated
551 with MIS 10. This Liviecian glaciation was the first glacial episode of the Saalian
552 Stage (s.s.) and preceded the Zbójnian Interglacial. During this event, the ice sheet
553 reached central Poland (Lindner and Marks 1999).

554

555 In Russia glacial deposits that have been reliably attributed to MIS 10 are very rare.
556 However, Astakhov (2004; 2011) suggested that a sequence found in Siberia possibly
557 represents a transition between Marine Isotope Stages (MIS) 10–9 where deep-marine
558 sedimentation resulting from isostatic loading from the previous phase of glaciation is
559 found. This dating is based on electron spin resonance (ESR) and green stimulated
560 luminescence (GSL) ages of 300–400 ka. Similar ages have been reported for marine
561 deposits from a few localities on the Taymyr Peninsula (Bolshiyarov et al., 1998). If
562 this interpretation is correct, then it implies the development of a substantial ice cap
563 over northern Siberia in MIS 10.

564

565 In North America, there is evidence of glacial advances into Pennsylvania during the
566 Middle Pleistocene (pre-Illinoian A or B—MIS 10 or 12; i.e. Early Saalian and
567 Elsterian) and overlain by late Middle Pleistocene (MIS 6—Illinoian or Late Saalian)
568 (using the terminology of Richmond and Fullerton, 1986) deposits (Braun, 2011).
569 Deposits possibly relating to MIS 10 may be present in the Stikine Valley in north-
570 western British Columbia where they underlie basalt dated by K-Ar to 300 ± 30 ka
571 (Spooner et al. 1996; Duk-Rodkin and Barendregt 2011).

572

573 In the southern hemisphere there is little evidence in the glacier record of MIS 10
574 glaciation. However, in the Western Arthur Range of southwestern Tasmania
575 cosmogenic exposure dating suggests that moraines were formed by glaciations in
576 MIS 6 and 10 but not in MIS 8 (Kiernan et al. 2010). However, Kiernan et al. (2010)
577 do acknowledge that the MIS 10 age may be an over-estimate if the erosion rates are
578 too high, and in that case the moraines would be MIS 8 in age.

579

580 **3.3. MIS 14**

581 MIS 14 was characterised by limited global ice extent. The signal of
582 climatic/environmental change is particularly weak in a range of records, marine and
583 terrestrial, leading Lang and Wolff (2011, p. 375) to argue that “it is sufficiently weak
584 that one could question its designation as a glacial”. In the marine isotope record the
585 maximum $\delta^{18}\text{O}$ value of this cold stage was 4.55 at 548 and 536 ka, which is the
586 lowest $\delta^{18}\text{O}$ value of all the last ten cold stages (Figure 4). Ice volume was the lowest
587 of all the last ten glacial-interglacial cycles with global sea levels much higher than in
588 other cold stages at -67.39 m at 537 ka (Table 1; Figure 4). Sea levels reached -62.75
589 m at 550 ka and remained depressed through to MIS 13b (-55.45 m), suggesting that
590 the definition of this glaciation spans a longer interval than just MIS 14, despite
591 termination IV being recorded in the marine isotope record and a sharp rise in global
592 sea-surface temperatures at this time (Figure 4). The start of MIS 14 was associated
593 with the strongest solar-trough magnitude of the last seven glacial-interglacial
594 cycles (Table 2). However, this was mitigated by the fact that preceding peak in
595 solar radiation (and median peak-trough value) was the largest solar peak at the
596 glacial inception of the last seven glacial-interglacial cycles. Despite the evidence
597 of limited global ice extent, global sea surface temperatures during MIS 14 were as
598 cold as other cold stages that were characterised by much bigger glaciations
599 (Shakun et al. 2015). The Antarctic dust signal for MIS 14 is much weaker than for
600 any other glacial-interglacial cycles with dust flux $< 12 \text{ mg/m}^2/\text{a}$. A double peak
601 pattern is evident at c. 540 and 530 ka with the first peak larger than the second
602 (Figure 4).

603

604 There is little direct evidence of glaciation on land from MIS 14, probably because
605 it was limited in extent compared to later glaciations. However, in the Italian
606 Apennines a glacier advance has been dated to MIS 14 by applying $^{36}\text{Ar}/^{40}\text{Ar}$

607 dating to tephra deposits in a pro-glacial lacustrine sequence in the Campo Felice
608 basin (Giraudi et al. 2011).

609

610 **3.4. The glaciations that didn't make it: MIS 7d, MIS 13b and 15b**

611 Some intervals characterised by major excursions in the marine oxygen isotope curve
612 do not fit the criteria for definition as glacial-interglacial cycles as set out in Hughes
613 and Gibbard (2018). Furthermore, they often do not conform to the conventional
614 “sawtooth” model of 100 ka glacial cycles, such as MIS 7d (Ruddiman and McIntyre
615 1982). They either do not end in formally defined terminations, are insufficiently cold
616 as recorded in proxies such as global SSTs, or have not been assigned full stage status
617 in the marine isotopic record. In Antarctic dust records from MIS 7d, 13b and 15b the
618 dust flux is relatively insignificant compared with full glacial-interglacial cycles.

619 Whilst Antarctic dust flux cannot be directly related to global ice volumes only
620 patterns of change, it nevertheless suggests that these intervals did not have
621 significant effects on the global hydrological cycle. However, MIS 7d, 13b and 15b
622 are each represented by high amplitude excursions of the $\delta^{18}\text{O}$ curve in the marine
623 isotope record and their magnitude stands out compared with other stadials within
624 glacial-interglacial cycles (Figure 4).

625

626 MIS 7d is the most pronounced of the three anomalous isotopic stadials (cf.
627 Ruddiman and McIntyre 1982) and had a $\delta^{18}\text{O}$ value almost as high as MIS 14 in the
628 stacked record of Lisiecki and Raymo (2006). In fact, in the sea-level stack of Spratt
629 and Lisiecki (2016) MIS 7d has a slightly lower sea level than MIS 14, at -68.74 m
630 (MIS 7d) versus -67.39 m (MIS 14) (Table 1; Figure 4). In other indicators such as
631 Shakun et al.'s (2015) global sea-surface temperature stack, MIS 7d is a significant
632 stadial but MIS 14 is much colder. In the same record both MIS 13b and 15b are
633 insignificant events yet they recorded global sea levels at -55.45 and -54.4 m,
634 respectively, and with large isotopic excursions in the marine $\delta^{18}\text{O}$ record (Figure 4).
635 This suggests that these glaciations represented large regional but not global
636 glaciation events. The very weak dust signal in the Antarctic ice core record also
637 suggests that these glaciation events were confined to the Northern Hemisphere
638 (Figure 4). In the Northern Hemisphere, very low arboreal pollen percentages in
639 southern Europe indicate that MIS 7d was associated with very dry and cold
640 conditions (Roucoux et al. 2008). This is associated with a major trough in Northern

641 Hemisphere summer radiation, the lowest of the past 800 kyr. The brevity of the
642 stadial is likely to be explained by the subsequent peak in solar radiation in the
643 Northern Hemisphere, which was the highest of the past 800 kyr (Figure 4).
644

645 The problem of defining glacial-interglacial cycles using the marine isotopic record is
646 further compounded by the recognition or non-recognition of terminations.
647 Technically, MIS 7d could be classified as part of a glacial-interglacial cycle based on
648 terminations because it is bounded by terminations III (243 ka) (McManus et al. 1999;
649 Lisiecki and Raymo 2006) and IIIa (225 ka) (Cheng et al. 2009). The age of IIIa at
650 225 ka, derived from U-series dating of a Chinese speleothem (Cheng et al. 2009),
651 differs from the marine isotope curve, which shows a typical sharp transition slightly
652 later at c. 219-220 ka. This may be an artefact of the age model used in the Lisiecki
653 and Raymo (2005) LR04 stack. In fact, Cheng et al. (2009) found that variations in
654 other marine isotopic records such as that at ODP 980 (McManus et al. 1999) were 3
655 kyr too young when compared with high resolution dated speleothem records.
656

657 MIS 7d represents an anomaly for the preceding and succeeding glacial-interglacial
658 cycles of MIS 9a-8 and MIS 6 because Hughes and Gibbard (2018) defined these
659 cycles as spanning terminations IV-III and IIIa-II, respectively. In this sense MIS 7d
660 and the interval between terminations III and IIIa represent a truly “missing”
661 glaciation if defined using terminations as the bounding criteria. The main
662 characteristic that defines MIS 7d as a stadial, rather than a full glacial, is its length,
663 which between terminations III and IIIa is just 18 ka, compared with 76-118 ka for
664 the last ten “full” glacial-interglacial cycles.
665

666 MIS 15b, 13b and 7d are associated with high or rising eccentricity and the associated
667 pronounced high-amplitude fluctuations in precession (Figure 4). The intervals began
668 with major solar troughs followed by equally large upswings in solar radiation
669 through 600-589 kyr and 230-220 kyr in the Northern Hemisphere. At the end of MIS
670 15b the Northern Hemisphere summer insolation reached one of the highest peaks of
671 the last million years. This pattern of solar radiation changes would have prevented
672 Northern Hemisphere ice-expansion achieving the magnitude reached during full
673 glacial-interglacial cycles. In the case of MIS 15, this pronounced insolation peak
674 would have also impacted on the development of the following glacial-interglacial

675 cycles encompassing MIS 14, as noted earlier. This highlights how important
676 Northern Hemisphere insolation is in driving glaciations and the structure of glacial-
677 interglacial cycles. Whilst Hughes and Gibbard (2018) found that changes in Northern
678 Hemisphere insolation accounts for *c.* 50-60% of global glacier changes, the rest is
679 accounted for in regional internal factors. However, that is for 100 kyr glacial-
680 interglacial cycles, and for short “missing” glacial intervals like MIS 15b,13b and 7d
681 the role of insolation is likely to be even more critical in preventing the development
682 of full glacial-interglacial cycles.

683

684 **4. Discussion**

685 **4.1. “Missing glaciations” – real or apparent?**

686 The hypothesis that global glacier extents were significantly more limited in some
687 glacial-interglacial cycles than others has been tested using a variety of different
688 records. The first and obvious place to look is in the terrestrial record and here
689 notably there is limited evidence of major global glacier extents in MIS 8, 10 and 14.
690 However, this is not to say that there is no evidence of glaciation in intervals such as
691 MIS 8, only that the patterns of global glaciation do not match those of other glacial-
692 interglacial cycles such as MIS 5d-2, 6 and 12. Indeed, in some areas like North-East
693 Asia and Patagonia MIS 8 was characterised by a major glacier advance. A key
694 challenge is understanding the true age of the pre-Illinoian glaciations in North
695 America, for which conclusive evidence remains elusive (Rovey and Balco 2011).
696 Nevertheless, most evidence here and in Europe points to MIS 6 being a larger
697 glaciation than both MIS 10 and 8 in most regions.

698

699 The terrestrial record of glaciations can potentially provide a misleading impression
700 of the extent of glaciations during different glacial-interglacial cycles, especially
701 where glacial limits were overridden by later glaciers. Even if this was the case, some
702 “missing glaciations” may have been characterised by ice extents that were similar in
703 size to those in later glaciations. However, MIS 8, 10 and 14 were all characterised by
704 much smaller global sea-level depressions, which supports the idea that these were
705 characterised by glaciers that were relatively limited in extent and volume compared
706 with other glacial-interglacial cycles. Dust records also provide insights into the
707 patterns of ice build-up in these glaciations compared with larger glaciations. In the
708 “missing glaciations”, dust peaks indicate an early global glacier advance that had

709 more impact on the global hydrological cycle than later in the glacial-interglacial
710 cycle. In the largest glaciations of MIS 5d-2, 6, 12 and 16, the dust peaks were
711 towards the end of glacial-interglacial cycles at the global glacial maxima. The early
712 dust peaks in these big glaciations appear to be associated with glacier advances in
713 high-latitude Asia and globally in the mid-latitude mountains, whereas the later dust
714 peaks correspond with maxima of the large continental ice sheets over North America
715 and Europe (Hughes and Gibbard 2018). In the “missing glaciations” it appears that
716 these early glacier advances had bigger impacts on Antarctic dust flux than the later
717 global glacial maxima. Thus, this analogue suggests that during the “missing
718 glaciations” of MIS 8, 10 and 14 the ice sheets of North America and Europe had
719 much less effect on Antarctic dust flux than in the more extensive glaciations of MIS
720 5d-2, 6, 12 and 16.

721

722 Whilst global glacier extents during MIS 8 and 10 are argued to have been less than in
723 other glacial-interglacial cycles, these intervals are associated with a large ice-rafted
724 debris (IRD) signal in North Atlantic marine sediment sequences (McManus et al.
725 1999). This is in contrast to the muted signal of the ‘Fleuve Manche’ fluvial
726 discharge through the English Channel during these glaciations (Figure 6). The large
727 IRD signals in MIS 8 and 10 are related to major fluctuations in high-latitude ice-
728 sheet margins around the North Atlantic, whereas the ‘Fleuve Manche’ signal is
729 related to ice-sheet margins further south in the mid-latitudes, Some of these margins
730 are associated with the same ice sheets, such as the British-Irish Ice Sheet. The
731 apparent contradiction of high IRD in the north-eastern Atlantic (McManus et al.
732 1999), yet limited fluvial discharge associated with ‘Fleuve Manche’ (Toucanne et al.
733 2009a) suggests a different ice configuration than in later glaciations. Whilst North
734 Atlantic IRD at sites further south and west than ODP 980 is usually dominated by a
735 North American source, background levels of IRD have been linked to the British-
736 Irish Ice Sheet (Bigg et al. 2010). On the continental margin offshore of Ireland,
737 radiogenic isotope source-fingerprinting, in combination with coarse lithic component
738 analysis, indicates a dominant IRD source from the British-Irish ice sheet since the
739 earliest Pleistocene (Thierens et al. 2012). It is therefore possible that the ice sheets
740 over Ireland and Scotland in MIS 8 and 10 were very active, possibly reaching the
741 Atlantic continental shelf as in the last glacial-interglacial cycle (Stoker and Bradwell
742 2005; Bradwell et al. 2007; Peters et al. 2016), but that this was not matched by

743 extensive ice further east over England and Wales or continental Europe. Thus, the
744 contrasting evidence for glaciation in MIS 8 and 10 from the high- and mid-latitudes
745 in the NE Atlantic region, as well as across the globe, hints at a major difference in
746 ocean-atmosphere configuration compared with other glacial-interglacial cycles.

747

748 The different ocean-atmosphere configurations in MIS 10 and 8 compared with other
749 glaciations in MIS 12, 6 and 5d-2 may be linked to ocean circulation in the North
750 Atlantic and especially North Atlantic deepwater formation. This is known to be
751 affected by the flux of water from the south (Gutjahr et al. 2010) and thus ice sheet-
752 ocean dynamics around Antarctica may have played a significant role in explaining
753 the instability of Northern Hemisphere ice masses in MIS 8 and 10. In fact, as noted
754 earlier, dust flux over Antarctica for MIS 8 was one of the largest and most sustained
755 of the last million years, reaching values comparable with MIS 6 and greater than in
756 MIS 5d-2. This may therefore indicate that global ice volume in MIS 8 was
757 dominated by Southern Hemisphere ice expansion. There is strong evidence of a large
758 glacier advance in Patagonia at *c.* 260 ka. However, elsewhere, in Australasia the
759 evidence for MIS 8 is not so clear, with glaciations MIS 6 and 10 appearing to be
760 larger. Hein et al. (2017, p. 93) wrote that the “cause of the large MIS 8 advance in
761 central Patagonia during a comparatively minor global ice age is unclear, and is an
762 avenue for future research”.

763

764 Evidence from the Stocking Glacier in the McMurdo Dry Valleys in Eastern
765 Antarctica shows that the glacier was 20-30% larger than today at 391 ± 35 ka, during
766 MIS 11 (Swanger et al. 2017). It also illustrates that the Dry Valleys have been ice-
767 free for at least the last 350-400 ka. This is important because it suggests that
768 expansion of the East Antarctic Ice Sheet cannot have been a major factor in
769 explaining differences between the last four 100 kyr glacial-interglacial cycles.
770 Instead, it is the smaller and more dynamic West Antarctic Ice Sheet that is most
771 likely to have varied between these glacial-interglacial cycles. West Antarctica is
772 surrounded by the largest area of continental shelf around the continent, with large
773 areas available for ice growth; much larger than around the East Antarctic ice sheet
774 relative to the current size of the respective ice sheets (Figure 7). The West Antarctic
775 Ice Sheet has long been considered to be prone to collapse (Mercer 1984; Pollard and
776 DeConto 2009). The shelf configuration around this region is equally likely to have

777 facilitated rapid and extensive ice build-up during periods of low global sea levels
778 during glaciations. After the Early-Middle-Pleistocene transition it has been suggested
779 that the West Antarctic Ice Sheet shifted to a marine-based configuration (Sutter et al.
780 2019), and it is likely that the nature of this configuration through different
781 subsequent glacial-interglacial cycles would have been a major factor in influencing
782 ice sheet dynamics. However, most glacial geological studies of the West Antarctic
783 Ice Sheet relate to the last glacial-interglacial cycle (e.g. Sugden et al. 2006) with little
784 direct evidence of Middle Pleistocene glacial histories.

785

786 Given the evidence above, any Southern Hemisphere lead associated with Antarctica,
787 must be associated with changes in the West Antarctic Ice Sheet. This is in terms of
788 both ice sheet-atmosphere and ice sheet-ocean interactions, the latter influencing
789 climate in the Northern Hemisphere through both the thermal ocean seesaw (Crowley
790 1992; Stocker and Johnsen 2003; Pedro et al. 2018) and the deep-water seesaw
791 (Broecker 1998). Increased freshwater input from ice sheets as they expanded to the
792 continental shelf causing greater calving loss is likely to have a major impact on
793 Antarctic Meridional Overturning Current which in turn affects the strength of North
794 Atlantic deep-water formation (Swingedouw et al. 2009).

795

796 Thus, extensive West Antarctic Ice Sheets in MIS 8 and 10 may have reduced the
797 strength of the North Atlantic Conveyor, inhibiting moisture delivery to the areas of
798 potential ice-sheet growth in lands bordering the North Atlantic Ocean. In this
799 scenario the early dust peak maxima in both MIS 10 and 8 (Figure 4) would be caused
800 by the Southern Hemisphere lead in ice build-up, which was matched by ice build-up
801 in the Northern Hemisphere, especially over Asia. However, as West Antarctic ice
802 grew larger through the glacial-interglacial cycle this caused a shutdown of the North
803 Atlantic Conveyor starving ice sheets around the North Atlantic Ocean of moisture,
804 explaining their absence from the geological record. This pattern is best suited to
805 explain the nature of glaciations in MIS 8 since the early dust peak is also matched by
806 the lowest global sea levels, which both precede the benthic $\delta^{18}\text{O}$ trough by c. 18 kyr.
807 Whilst MIS 10 exhibited some similarities to MIS 8, it also had similarities with the
808 larger glacier extents of MIS 12, 6 and 5d-2. MIS 14, on the other hand, has strong
809 similarities with MIS 8, especially since both are followed by extended interglacial
810 complexes (MIS 13 and 7, respectively). Hao et al. (2015) argued that MIS 14

811 inception was a response to changes in Antarctic ice sheets rather than to Northern
812 Hemisphere cooling. However, in MIS 14 it is likely that the West Antarctic Ice
813 Sheet was more restricted and sensitive than in MIS 10 and 8 since there is evidence
814 that the ice sheet collapsed in the interval MIS 15-13 (Hillenbrand et al. 2009). This is
815 possibly due to significantly higher global sea levels during MIS 14 than occurred in
816 other major glaciations (Table 1).

817

818 The relatively weak signal of global glaciation within MIS 14 has also been
819 proposed as a direct cause of the extended interglacial complex of MIS 15-13 (Hao
820 et al. 2015). Whilst the strong solar radiation peak that preceded this glaciation in
821 MIS 15a would have mitigated glacier inception in MIS 14, the subsequent weak
822 global glaciation would also have an impact on the extended interglacial that
823 followed (MIS 13). This is also evident in the case of MIS 8, a weak global
824 glaciation which was followed by the extended interglacial complex of MIS 7. This
825 observation also has relevance for subsequent glacial inception, with some cases of
826 failed glacial-interglacial cycles evident in intervals such as MIS 13b and 7d, which
827 succeeded the weak glaciations in MIS 14 and 8, respectively.

828

829 **4.2. Looking for patterns: the role of orbital forcing in explaining the** 830 **magnitude of glaciations**

831 There is a clear link between the magnitude of peak-trough variations at the end of
832 interglacials and the intensity of global glaciations in the subsequent cold stage. This
833 is evident in the values of solar-trough magnitude for the last seven glacial-
834 interglacial cycles (Table 2). MIS 8 and 10 are associated with the lowest values of
835 solar-trough magnitude. Lower solar-trough magnitudes at the end of interglacials
836 means that glacier build-up early in the glacier cycles is likely to be less significant
837 than in other glacial-interglacial cycles where solar-trough magnitudes are more
838 pronounced (Table 2). MIS 14 does not follow conform with this theory since it was
839 characterised by a large solar-trough magnitude at the end of MIS 15. However, the
840 preceding solar radiation peak was the largest preceding any of the last seven glacial-
841 interglacial cycles and was associated with maximum eccentricity (Figure 4). In fact,
842 in the last 800 kyr solar radiation only exceeded the MIS 15/14 peak in the Northern
843 Hemisphere summer in the extended interglacial complex of MIS 7 (Figure 4).

844

845 As noted earlier, the drivers of global glacial dynamics during the weaker global
846 glaciations in MIS 8 and 14 appear to have had a southern lead, and to be dominated
847 by changes in Antarctic ice sheets rather than to Northern Hemisphere cooling. This
848 suggests that a Northern Hemisphere lead in driving global glaciations through solar
849 forcing is mitigated by interhemispheric ocean-atmospheric connections (Table 2).
850 This partly explains why changes in Northern Hemispheric solar radiation can only
851 explain 50-60% of global ice volume through the last 100 kyr glacial-interglacial
852 cycles (cf. Hughes and Gibbard 2015). The evidence also suggests that changes in
853 Northern Hemispheric solar radiation have a much smaller influence in explaining
854 glacier dynamics during the “missing glaciations”, such as MIS 8 and 14. Whilst there
855 was a northern lead and quasi-synchronicity in climate for the most severe and largest
856 glaciations of MIS 16, 12, 6 and 5d-2, driven by changes in solar radiation input to the
857 Northern Hemisphere (e.g. Mercer 1984), this was not the case for the “missing
858 glaciations” of MIS 14, 10 and 8. This is important because it shows that solar forcing
859 was not a significant control on global glaciation during the “missing glaciations”. It
860 illustrates that the Milankovitch hypothesis cannot explain the structure of all glacial
861 cycles – a point noticed several decades ago (see references in Mercer 1984). This is
862 still a significant issue today since the marine isotope record is still tuned to the
863 pacing of orbital variations (Lisiecki and Raymo 2006) following the findings of Hays
864 et al. (1976). Whilst this is appropriate for the classic 100 ka glacial cycles such as
865 MIS 16, 12, 6 and 5d-2 the efficacy of orbital tuning breaks down when dealing with
866 “missing glaciations” such as MIS 14, 10 and 8. This, and the fact that the marine
867 oxygen isotope record suffers from spatial bias (i.e. the dominance of the Laurentide
868 Ice Sheet), means that the established view of glacial-interglacial cycles through the
869 lens of the marine isotopic curve can be misleading.

870

871 There is a potential link between orbital eccentricity and the magnitude of glaciations
872 over the last five glacial-interglacial cycles. Increasing eccentricity causes increasing
873 amplitude of variations in the climatological precession parameter ($e \sin \omega$) that
874 describes how the precession of the equinoxes affects the seasonal configuration of
875 the Earth-Sun distance (Berger and Loutre, 1991, p. 297). This affects the solar-
876 trough magnitude at the end of interglacials (Figure 4). Small glaciers can rapidly
877 build-up in response to mass balance changes associated with a deteriorating climate

878 (Bahr et al. 1998). This explains why mountain glaciers are often seen to reach their
879 maxima early in glacial-interglacial cycles when precession contrasts are at their
880 greatest (see Hughes et al. 2013; Hughes and Gibbard 2018). However, precessional
881 cycles are too short to sustain larger ice sheet build-up. This means that ice sheets are
882 more likely to sustain build-up during periods of low precessional variability. This
883 was the case in MIS 12 for example (Figure 4). Another important consideration is the
884 effect of diminishing magnitude of precessional cycles through glacial-interglacial
885 cycles, which is displayed during some of the largest glaciations such as in MIS 12
886 and 5d-2 (Figure 4). In contrast, this effect is much weaker or reversed (i.e. increasing
887 magnitude of precessional cycles) during MIS 8 and 10, respectively. Diminishing
888 precession results in excess ice build-up causing ice sheet instability and collapse
889 during terminations after the fourth or fifth precessional cycles (Raymo 1997;
890 Ridgwell et al. 1999). This is because diminished precession causes smaller changes
891 between the seasons and the negative effects on glacier mass balance of the
892 lengthening of the melt season during upswings to solar peaks is reduced (Hughes and
893 Gibbard 2018).

894

895 The sets of consecutive “missing glaciations” in MIS 10 and 8 occurred during a trend
896 towards increasing eccentricity and precession which caused larger amplitude
897 variations in solar radiation, which reached their greatest amplitude in MIS 7 (Figure
898 4). Other “missing glaciations” in the weak pseudo-glacial-interglacial cycles of MIS
899 7d, 13b and 15b also correspond with large amplitude solar cycles associated with
900 increased eccentricity and associated precession. This pattern supports the idea that
901 glaciations are influenced by 413 kyr cycles with 100 kyr glacial-interglacial cycles
902 superimposed and modulated by these larger-scale orbital cycles (Rial 1999).
903 However, the relationship is not perfect because MIS 16, one of the major global
904 glaciations, also occurred during a rising trend of eccentricity (Figure 4). However,
905 this earlier eccentricity cycle was less pronounced than that which occurred over the
906 last five glacial-interglacial cycles and the effects on precession were smaller.

907

908 **4.3. “Missing glaciations” and implications for Quaternary** 909 **chronostratigraphy**

910 The fact that not all 100 kyr glacial-interglacial cycles produced the same magnitude
911 of ice extent and volume on Earth has major implications for understanding how these

912 cycles relate to glaciations. This is complicated further when considering shorter term
913 climatic variations and their global glacier imprint. For example, despite being
914 classified within isotope interglacials, MIS 7d and 15b saw global sea-level
915 depressions similar to some glacier maxima within full glacial-interglacial cycles.
916 This highlights the problems of using single proxy records, largely dominated by the
917 marine isotope record, as a measure of the extent and pacing of global glaciations.
918 The fact that marine isotope sequences are tuned by orbital parameters provides a
919 sense of regularity around glacial-interglacial cycles when it is apparent that not all
920 glacial-interglacial cycles are the same, with some very different to others. The lesson
921 from this is that the extent and magnitude of glaciations within glacial-interglacial
922 cycles cannot be deciphered using the marine isotope record alone. This further
923 highlights the problems of correlating terrestrial sequences with the marine isotope
924 record (cf. Gibbard and West 2000) and is a problem not limited to just glacier
925 records (e.g. Biñka and Marks 2018).

926

927 For example, for one of the most extensive glaciations of the Quaternary, the Saalian,
928 Wolstonian, Illinoian and equivalents (during MIS 6), both the timing and extent of
929 individual regional glacial advances and retreats vary significantly. In northern
930 Europe, two major stadial advances are recognised during the classical Saalian
931 glaciation, the Late Saalian Drenthe and Warthe Stadial advances, lasting from ~180-
932 160 and 150-140 ka, respectively (Toucanne et al. 2009a; Margari et al. 2014). In the
933 past, these events had been thought to represent separate glaciations, however, there is
934 no evidence of major interstadial or interglacial warming during the intervening
935 interval (Ehlers et al. 2011c). Whilst robust dating now indicates that the two major
936 intervals occurred during the same glaciation, marine records indicate that after ~150
937 ka ice sheets expanded, with global ice volume reaching the Penultimate Glacial
938 Maximum (PGM) extent towards the end of MIS 6 (i.e. ~140 ka). This principally
939 reflects the growth of the late Illinoian ice sheet in North America (e.g. Curry, et al.
940 2011; Syverson and Colgan, 2011; Margari et al. 2014). However, in Europe the
941 equivalent Warthe ice advance was markedly less extensive than the Drenthe/Dniepr,
942 although this might have been compensated for by glacial expansion in Russia and
943 Siberia (e.g. Astakhov, 2004). Likewise, the apparent absence of glaciation during
944 MIS 8 (Middle Saalian/pre-Illinoian A) in both western Europe in North America

945 contrasts with the record in the east, such as in Siberia, where the ice reached its
946 Pleistocene maximum extent at that time.

947

948 In recent publications on the Quaternary stratigraphy of northern Germany, and to
949 some extent elsewhere, references to the correlation with marine isotope stages are
950 largely avoided. The number of interglacials between Elsterian and Saalian is still
951 disputed, but the position of the Holsteinian Stage interglacial has gradually moved
952 from MIS 7 (Caspers et al., 1995), via MIS 9 (Litt et al., 2007), to MIS 11 (Ehlers,
953 2011, Stephan, 2014). If the latter interpretation is correct, except for the Trelidenæs
954 Till in Jutland (Denmark), no truly glacial deposits of either MIS 10 or 8 have been
955 identified so far. In the British Isles, the equivalent of the Saalian Stage interval is
956 defined as the Wolstonian in a borehole at Marks Tey in East Anglia. As in Germany
957 (cf. Stephan 2014), the Wolstonian Stage has been plagued by incorrect correlations
958 with the marine isotopic record because of the climatic complexity within it. This is
959 despite Gibbard and Turner (1990) stating that “the Wolstonian Stage includes all
960 time between the end of the Hoxnian [~MIS 11] and the beginning of the Ipswichian
961 [~MIS 5] Stages irrespective of climatic or similar events that may be subsequently
962 identified”. The evidence presented in here shows that whilst there is no doubt that
963 multiple such climatic and glaciation events occurred in MIS 10 and 8, their imprint
964 in the terrestrial sequences is frequently lacking and this highlights why glaciations
965 are time-transgressive events and should not be confused with true
966 chronostratigraphical units in the Quaternary stratigraphical record.

967

968 Another consequence of the observations presented here is that for older glaciations,
969 in common with those of the last glacial-interglacial cycle (Weichselian,
970 Wisconsinan, Valdaian, etc.; Hughes et al. 2013; Hughes & Gibbard 2018), it cannot
971 be assumed that ice sheets throughout the world reached their maximum extents at the
972 same time. Rather it appears that asynchronicity is the norm, at least during the major
973 glaciations of the Middle to Late Pleistocene. All these results clearly emphasise the
974 danger of adopting a simplistic counting backward-and-forward approach to extra-
975 regional glacial stratigraphy. Indeed the implications for stratigraphical and
976 modelling reconstructions are profound. The lesson being that simple, one-to-one,
977 uncritical correlations with terrestrial, and in particular with the marine isotope
978 sequences, hold numerous potentially serious pitfalls for the unwary.

979

980 **5. Conclusions**

981 Glaciations in MIS 8 and 10 were relatively limited in extent in western Europe and
982 North America, in comparison to other Middle Pleistocene glaciations such as the
983 Elsterian/pre-Illinoian B (MIS 12) and the Late Saalian/Illinoian (MIS 6). MIS 14 is
984 notable for being especially marginal as a glacial-interglacial cycle compared with
985 other 100 kyr cycles in terms of glacier extent and related global climatic and
986 environmental indicators. In most areas glaciations were less extensive in MIS 8, 10
987 and 14 than the Weichselian/Wisconsinan (MIS 5d-2), with a few notable exceptions.
988 For example, east of the Urals in Siberia, the maximum extent of MIS 8 glaciation
989 marks the maximum extent of Pleistocene glaciation in this region. Also, in parts of
990 Patagonia, MIS 8 glaciers were larger than in both MIS 6 and 5d-2.

991

992 The records for MIS 8 and 10 differ from other glacial-interglacial cycles in that there
993 is evidence for pronounced dust peaks in Antarctic ice cores early on with smaller
994 dust peaks towards the end of the glacial-interglacial cycles during global glacier
995 maxima. The early dust peak in the last glacial-interglacial cycle (MIS 5d-2) is
996 associated with early advances of glaciers in the mid-latitude mountains, continental
997 interiors, and especially Arctic Asia and in mountains bordering the NW Pacific
998 Ocean (Batchelor et al. 2019). By analogy, this implies that MIS 8 and 10 saw large
999 glaciations in these regions but less significant continental ice sheet expansions
1000 around the North Atlantic margins. This is supported by sea-level evidence, with
1001 global sea-level depressions 20-30 m less in MIS 8 and 10 compared to that during
1002 MIS 12, 6 and 2. However, early dust peaks in MIS 8 are also closely related to
1003 significant ice expansion in Patagonia suggesting a Southern-Hemisphere lead. The
1004 relationship between Southern and Northern Hemisphere glaciations is likely to be
1005 affected by the dynamics of the West Antarctic Ice Sheet and the effects of its
1006 expansion on ocean circulation through oceanic bipolar seesaws.

1007

1008 Solar forcing plays a major role in determining the size and length of glaciations.
1009 Over the long term, the “missing glaciations” of the last five glacial-interglacial
1010 cycles are associated with rising eccentricity and increased precession. Whilst this
1011 accelerates glacier build-up in the short term during pronounced insolation downturns,
1012 it hinders their build-up during the following upswing. For example, the amplitude of

1013 solar precession associated with peak eccentricity can be linked to failed glacial-
1014 interglacial cycles such as MIS 7d and 15b. These short intense stadials were
1015 prevented from developing into full glacial-interglacial cycles directly because of the
1016 pattern of Northern Hemisphere solar variations.

1017

1018 The fact that 100 kyr glacial-interglacial cycles produced glaciations of very different
1019 magnitudes in different places around the globe poses problems when relying on a
1020 global indicator of glacier change, as is often the case when using the marine isotopic
1021 record. This has important implications for using the marine isotope record as a basis
1022 for understanding glaciations on land and wider terrestrial records. The structure of
1023 glacial-interglacial cycles, whilst predictable when considering the largest glaciations,
1024 is much less clear when considering weaker global glaciations in MIS 8, 10 and 14.
1025 The spatial and temporal patterns of glaciation were different in these glacial-
1026 interglacial cycles compared to the strongest glaciations of the last 500 kyr in MIS 12,
1027 6 and 5d-2. This indicates that glacial-interglacial cycles are not as predictable as is
1028 suggested in marine isotopic records that are tuned by orbital cycles.

1029

1030 **Acknowledgements**

1031 We thank Editor Nicholas Lancaster, Associate Editor Pat Bartlein and two
1032 anonymous reviewers for detailed and very helpful comments on an initial draft of
1033 this paper. We also thank Graham Bowden and Nick Scarle for drawing the figures.

1034

1035 **References**

1036

1037 Arndt, J.E., H. W. Schenke, M. Jakobsson, F. Nitsche, G. Buys, B. Goleby, M.
1038 Rebesco, F. Bohoyo, J.K. Hong, J. Black, R. Greku, G. Udintsev, F. Barrios, W.
1039 Reynoso-Peralta, T. Morishita, R. Wigley, "The International Bathymetric Chart of
1040 the Southern Ocean (IBCSO) Version 1.0 - A new bathymetric compilation covering
1041 circum-Antarctic waters", 2013, *Geophysical Research Letters*, Vol. 40, p. 3111-
1042 3117, [doi: 10.1002/grl.50413](https://doi.org/10.1002/grl.50413)

1043

1044 Astakhov, V., 2004. Pleistocene ice limits in Russian northern lowlands. In: Ehlers, J.,
1045 Gibbard, P.L. (Eds.), *Quaternary Glaciations - Extent and Chronology. Part 1:*
1046 *Europe*. Elsevier, Amsterdam, p. 309-319.

1047
1048 Astakhov, V., 2011. Ice margins of northern Russia revisited. In: Ehlers, J., Gibbard,
1049 P.L., Hughes, P.D., (Eds). In: Ehlers, J., Gibbard, P.L. and Hughes, P.D. (Eds)
1050 Quaternary Glaciations - Extent and Chronology, Part IV - A Closer Look.
1051 Amsterdam: Elsevier. p. 1-14.
1052
1053 Astakhov, V., Shkatova, V., Zastrozhnov, A., Chuyko, M., 2016.
1054 Glaciomorphological map of the Russian Federation. Quaternary International 420, 4-
1055 14.
1056
1057 Bahr, D.B., Pfeffer, W.T., Sassolas, C., Meier, M.F., 1998. Response time of glaciers
1058 as a function of size and mass balance:1. Theory. Journal of Geophysical Research
1059 103, 9777-9782.
1060
1061 Barendregt and Duk-Rodkin 2011. Chronology and Extent of Late Cenozoic Ice
1062 Sheets in North America: A Magnetostratigraphical Assessment. In: Ehlers, J.,
1063 Gibbard, P.L., Hughes, P.D. (Eds.), Quaternary Glaciations - Extent and Chronology:
1064 A Closer Look. Developments in Quaternary Science, 15. Elsevier, Amsterdam, pp.
1065 419-426.
1066
1067 Barrell, D.J.A., 2011. Quaternary Glaciers of New Zealand. In: Ehlers, J., Gibbard,
1068 P.L., Hughes, P.D. (Eds.), *Quaternary Glaciations – Extent and Chronology – A*
1069 *Closer Look*. Developments in Quaternary Sciences, Elsevier, vol. 15, pp. 1047–1064.
1070
1071 Barrows, T.T., Stone, J.O., Fifield, L.K., Cresswell, R.G., 2002. The timing of the last
1072 glacial maximum in Australia. Quaternary Science Reviews 21, 159-173.
1073
1074 Batchelor, C.L., Margold, M., Krapp, M., Murton, D.K., Dalton, A.S., Gibbard, P.L.,
1075 Stokes, C.R., Murton, J.B., Manica, A., 2019. The configuration of Northern
1076 Hemisphere ice sheets through the Quaternary. Nature Communications 10:3713.
1077 <https://doi.org/10.1038/s41467-019-11601-2>.
1078

1079 Beets, D., Meijer, T., Beets, C., Cleveringa, P., Laban, C., van der Spek, A., 2005.
1080 Evidence for a middle Pleistocene glaciation of MIS 8 age in the southern North Sea.
1081 Quaternary International 133–134, 7–19.
1082
1083 Berger, A., 1992, Orbital Variations and Insolation Database. IGBP PAGES/World
1084 Data Center for Paleoclimatology Data Contribution Series # 92-007. NOAA/NGDC
1085 Paleoclimatology Program, Boulder CO, USA.
1086
1087 Berger, A., Loutre, M.F., 1991. Insolation values for the climate of the last 10 million
1088 years. Quaternary Sciences Reviews 10, 297-317.
1089
1090 Bigg, G.R., Levine, R.C., Clark, C.D., Greenwood, S.L., Hafliðason, H., Hughes,
1091 A.L.C., Nygård, A., Sejrup, H.P., 2010. Last glacial ice-rafted debris off soujtwestern
1092 Europe: the role of the British-Irish Ice Sheet. Journal of Quaternary Science 25, 689-
1093 699.
1094
1095 Biňka, K., Marks, L., 2018. Terrestrial versus marine archives: biostratigraphical
1096 correlation of the Middle Pleistocene lacustrine records from central Europe and their
1097 equivalents in the deep-sea cores from the Portuguese margin. Geological Quarterly
1098 62, 69-80. doi: 10.7306/gq.1395
1099
1100 Bintanja, R., Roderik, S.W., van de Wal, O.J., 2005. Modeled atmospheric
1101 temperatures and global sea levels over the past million years, Nature, 437, 125-128.
1102
1103 Bolliger, T., Feijfar, O., Graf, H.R. & Kalin, D.W. 1996. Vorläufige Mitteilung über
1104 Funde von pliozanen Kleinsäugetern aus den Höheren Deckenschottern des Irchels (Kt.
1105 Zürich). Eclogae geologicae Helvetiae 89, 1043–1048.
1106
1107 Bolshiyarov, D.Y., Savatuygin, L.M., Shneider, G.V., Molodkov, A.N., 1998. New
1108 data about modern and ancient glaciations of the Taimyro-Severozemlskaya region.
1109 Materialny glyatchiologicheskich issledovanii 85, 219-222 (in Russian).
1110

1111 Bradwell, T., Stoker, M., Larter, R. 2007. Geomorphological signature and flow
1112 dynamics of the Minch palaeo-ice stream, NW Scotland. *Journal of Quaternary*
1113 *Science* 22, 609–617.
1114

1115 Braun, D. 2011. The glaciation of Pennsylvania, USA. In: Ehlers, J., Gibbard, P.L.,
1116 Hughes, P.D. (Eds.), *Quaternary Glaciations - Extent and Chronology: A Closer*
1117 *Look*. *Developments in Quaternary Science*, 15. Elsevier, Amsterdam, pp. 521–530.
1118

1119 Bridgland, D.R., Howard, A.J., White, M.J., White, T.S. (eds) (2014): *Quaternary of*
1120 *the Trent*. Oxbow Books, Oxford, 416 pp.
1121

1122 Broecker, W.S., 1998. Paleocean circulation during the last deglaciation: a bipolar
1123 seesaw? *Paleoceanography* 13, 119-121.
1124

1125 Broecker, W.S., van Donk, J., 1970. Insolation changes, ice volumes, and the O¹⁸
1126 record in deep-sea cores. *Reviews of Geophysics* 8, 169–198.
1127

1128 Calvet, M., 2004. The Quaternary glaciations of the Pyrenees. In: Ehlers, J. and
1129 Gibbard, P. L. (editors): *Quaternary Glaciations – Extent and Chronology. Part I,*
1130 *Europe*. *Developments in Quaternary Science* 2, 119–128. Amsterdam, Elsevier.
1131

1132 Caspers, G., Jordan, H., Merkt, J., Meyer, K.-D., Müller, H, Streif, H., 1995.
1133 Niedersachsen. In: Benda, L. (Ed.), *Das Quartär Deutschlands*, Stuttgart,
1134 Borntraeger, 23-58.
1135

1136 Cheng, H., Edwards, L., Broecker, W.S., Denton, G.H., Kong, X., Wang, Y., Zhang,
1137 R., Wang, X., 2009. Ice Age Terminations. *Science* 326, 248-252, doi:
1138 10.1126/science.1177840
1139

1140 Claquin, T., Roelandt, C., Kohfeld, K., Harrison, S., Tegen, I., Prentice, I.,
1141 Balkanski, Y., Bergametti, G., Hansson, M., Mahowald, N., Rodhe, H., Schulz, M.,
1142 2003. Radiative forcing of climate by ice-age atmospheric dust. *Climate Dynamics*
1143 20, 193-202.

1144 Clark, P.U., Pollard, D., 1998. Origin of the Middle Pleistocene Transition by ice
1145 sheet erosion of regolith. *Paleoceanography* **13**, 1–9.

1146

1147 Cohen, K.M., Gibbard, P., 2011. Global chronostratigraphical correlation table for the
1148 last 2.7 million years. Subcommission on Quaternary Stratigraphy (International
1149 Commission on Stratigraphy), Cambridge, England.

1150 <http://quaternary.stratigraphy.org/charts/>

1151

1152 Colhoun, E.A., 1985. The Glaciations of the West Coast Range, Tasmania.
1153 *Quaternary Research* **24**, 39-59.

1154

1155 Colhoun, E.A., Barrows, T.T., 2011. The glaciation of Australia. In: Ehlers, J.,
1156 Gibbard, P.L., Hughes, P.D. (Eds.), *Quaternary Glaciations – Extent and Chronology*
1157 *– A Closer Look*. *Developments in Quaternary Sciences*, Elsevier, vol. 15, pp. 1037–
1158 1045.

1159

1160 Crowley, T., 1992. North Atlantic deepwater cools the Southern Hemisphere.
1161 *Paleoceanography* **7**, 489-497.

1162

1163 Curry, B.B., Grimley, D.A. & McKay, E.D. III, 2011, Quaternary glaciations in
1164 Illinois, in Ehlers, J., Gibbard, P.L. & Hughes, P.D., eds, *Quaternary Glaciations -*
1165 *Extent and Chronology - A Closer Look: Developments in Quaternary Science* **15**, p.
1166 467-487.

1167

1168 Davies, B.J., Roberts, D.H., Bridgland, D.R., Ó Cofaigh, C., Riding, J.B., Demarchi,
1169 B., Penkman, K., Pawley, S.M., 2012. Timing and depositional environments of a
1170 Middle Pleistocene glaciation of northeast England: New evidence from Warren
1171 House Gill, County Durham. *Quaternary Science Reviews* **44**, 180-212.

1172

1173 Demuro, M., Froese, D., Arnold, L., Roberts, R. 2012. Single-grain OSL dating of
1174 glaciofluvial quartz constrains Reid glaciation in NW Canada to MIS 6. *Quaternary*
1175 *Research*, **77**(2), 305-316.

1176

1177 Doppler, G., Kroemer, E., Rögner, K., Wallner, J., Jerz, H. & Grotenthaler, W. 2011.

1178 Quaternary Stratigraphy of Southern Bavaria. *E & G Quaternary Science Journal*

1179 60(2-3), 329-365.

1180

1181 Duk-Rodkin, A., Barendregt, R.W., Froese, D.G., Weber, F., Enkin, R.J., Smith, I.R.,

1182 Zazula, G.D., Waters, P., Kalssen, R., 2004. Timing and extent of Plio-Pleistocene

1183 glaciations in North-Western Canada and East-Central Alaska. In: Ehlers, J., Gibbard,

1184 P.L. (Eds.), *Quaternary Glaciations—Extent and Chronology. Part II: North America.*

1185 Elsevier, Amsterdam, pp. 313–345.

1186

1187 Duk-Rodkin, A., Barendregt, R.W., 2011. Stratigraphical record of

1188 glacials/interglacials in Northwest Canada. In: Ehlers, J., Gibbard, P.L., Hughes, P.D.

1189 (Eds.), *Quaternary Glaciations – Extent and Chronology – A Closer Look.*

1190 *Developments in Quaternary Sciences*, Elsevier, vol. 15, pp. 661–698.

1191

1192 Dyke, A.S., Prest, V.K., 1987. Late Wisconsinan and Holocene History of the

1193 Laurentide Ice Sheet". *Géographie Physique et Quaternaire*. 41, 237-263.

1194

1195 Ehlers, J., 2011. *Das Eiszeitalter*. Spektrum, Heidelberg. 372 pp.

1196

1197 Ehlers, J., Gibbard, P.L., Hughes, P.D. (Eds) 2011a. *Quaternary Glaciations - Extent*

1198 *and Chronology, Part IV - A Closer Look*. Amsterdam: Elsevier. 1108 pp.

1199

1200 Ehlers, J., Gibbard, P.L., Hughes, P.D. 2011b. *Quaternary Glaciations - Extent and*

1201 *Chronology, Part IV - a closer look: Introduction*. In: Ehlers, J., Gibbard, P.L. and

1202 Hughes, P.D. (Eds) *Quaternary Glaciations - Extent and Chronology, Part IV - A*

1203 *Closer Look*. Amsterdam: Elsevier. p. 1-14.

1204

1205 Ehlers, J., Grube, A., S. H-J., Wansa, S., 2011c. Pleistocene glaciations of North

1206 Germany – New Results. In: Ehlers, J., Gibbard, P.L. and Hughes, P.D. (Eds.),

1207 *Quaternary Glaciations – Extent and Chronology: A Closer Look*. *Developments in*

1208 *Quaternary Science*, 16. Elsevier: Amsterdam. p. 149-162.

1209

1210 Ehlers, J., Gibbard, P.L., Hughes, P.D., 2018. Quaternary glaciations and chronology.
1211 In: Menzies, J., van der Meer, J.J.M., (Eds). Past Glacial Environments. Elsevier. 2nd
1212 Edition. p. 77-101.
1213
1214 Elderfield, H., Ferretti, P., Greaves, M., Crowhurst, S., McCave, N., Hodell, D.,
1215 Piotrowski, A.M., 2012. Evolution of Ocean Temperature and Ice Volume Through the
1216 Mid-Pleistocene Climate Transition. *Science* 337, 704-709.
1217
1218 Evans, D.J.A., Roberts, D.H., Bateman, M.D., Ely, J., Medialdea, A., Burke, M.J.,
1219 Chiverrell, R.C., Clark, C.D., Fabel, D., 2019. A chronology for North Sea Lobe
1220 advance and recession on the Lincolnshire and Norfolk coasts during MIS 2 and 6.
1221 *Proceedings of the Geologists' Association*.
1222 <https://doi.org/10.1016/j.pgeola.2018.10.004>
1223
1224 Fernández Mosquera, D., Marti, K., Vidal Romaní, J.R., Weigel, D., 2000. Late
1225 Pleistocene deglaciation chronology in the NW of the Iberian Peninsula using cosmic-
1226 ray produced ²¹Ne in quartz. *Nuclear Instruments and Methods in Physical Research*
1227 *B* 172, 832–837
1228
1229 Fiebig, M., Ellwanger, D., Doppler, G., 2011. Pleistocene Glaciations of Southern
1230 Germany. In: Ehlers, J., Gibbard, P.L. and Hughes, P.D. (Eds) *Quaternary Glaciations*
1231 *- Extent and Chronology, Part IV - A Closer Look*. Amsterdam: Elsevier. p. 163-174.
1232
1233 Fitzsimons, S.J., Colhoun, E.A., van de Geer, G., 1990. Middle Pleistocene glacial
1234 stratigraphy at Baxter Rivulet, western Tasmania, Australia. *Journal of Quaternary*
1235 *Science* 5, 17-27.
1236
1237 Fitzsimons, S.J., Colhoun, E.A., van de Geer, G., Pollington, M., 1992. The Quaternary
1238 geology and glaciation of the King Valley. *Geological Survey Bulletin* 68, 1-57
1239 Tasmanian Department of Mines, Hobart.
1240
1241 Fletcher, W.J., Müller, U.C., Koutsodendris, A., Christanis, K., Pross, J. 2013. A
1242 centennial-scale record of vegetation and climate variability from 312 to 240ka

1243 (Marine Isotope Stages 9c-a, 8 and 7e) from Tenaghi Philippon, NE Greece.
1244 Quaternary Science Reviews 78, 108-125.
1245
1246 Fullerton, D.S., Colton, R.B., Bush, C.A., 2004. Limits of mountain and continental
1247 glaciations east of the Continental Divide in northern Montana and north-western
1248 North Dakota, U.S.A. In: Ehlers, J., Gibbard, P.L. (Eds.), Quaternary Glaciations -
1249 Extent and Chronology. Part 2: North America. Elsevier, Amsterdam, p. 131-150.
1250
1251 Ganopolski, A., Winkelmann, R., Schellnhuber, H.J., 2016. Critical insolation–CO₂
1252 relation for diagnosing past and future glacial inception. Nature 529, 200-203.
1253
1254 Ganopolski, A., Calov, R., 2011. The role of orbital forcing, carbon dioxide and
1255 regolith in 100 kyr glacial cycles. Climate of the Past 7, 1415–1425.
1256
1257 Gibbard, P.L., Turner, C., 1990. Cold stage type sections: some thoughts on a difficult
1258 problem. Quaternaire 1, 33-40.
1259
1260 Gibbard, P.L., West, R.G. 2000. Quaternary chronostratigraphy: the nomenclature of
1261 terrestrial sequences. Boreas 29, 329-336.
1262
1263 Gibbard, P.L., Clark, C.D., 2011. Pleistocene Glaciation Limits in Great Britain. In:
1264 Ehlers, J., Gibbard, P.L. and Hughes, P.D. (Eds) Quaternary Glaciations - Extent and
1265 Chronology, Part IV - A Closer Look. Amsterdam: Elsevier. p. 75-94.
1266
1267 Gibbard, P.L., West, R.G., Hughes, P.D., 2018. Pleistocene glaciation of Fenland,
1268 England, and its implications for evolution of the region. Royal Society Open Science
1269 4, 170736. <http://dx.doi.org/10.1098/rsos.170736>.
1270
1271 Gillespie, A., Molnar, P., 1995. Asynchronous maximum advances of mountain and
1272 continental glaciers. Reviews of Geophysics 33, 311-364.
1273
1274 Gillespie, A.R., Zehfuss, P.H., 2004. Glaciations of the Sierra Nevada, California,
1275 USA. In: Ehlers, J., Gibbard, P.L. (Eds.), Quaternary Glaciations - Extent and
1276 Chronology. Part 2: North America. Elsevier, Amsterdam, p. 131-150.

1277
1278 Gillespie, A.R., Clark, D.H., 2011. Glaciations of the Sierra Nevada, California, USA.
1279 In: Ehlers, J., Gibbard, P.L. and Hughes, P.D. (Eds) *Quaternary Glaciations - Extent*
1280 *and Chronology, Part IV - A Closer Look*. Amsterdam: Elsevier. p. 447-462.
1281
1282 Giraudi, C. and Giaccio, B., 2017. Middle Pleistocene glaciations in the Apennines,
1283 Italy: new chronological data and preservation of the glacial record. Geological
1284 Society, London, Special Publications, 433, 161-178.
1285
1286 Giraudi, C., Bodrato, G., Ricci Lucchi, M., Cipriani, N., Villa, I.M., Giaccio, B.,
1287 Zuppi, G.M., 2011. The Middle and late Pleistocene glaciations in the Campo Felice
1288 basin (Central Apennines, Italy). *Quaternary Research* 75, 219-230.
1289
1290 Graham, A.G.C., 2007. Reconstructing Pleistocene Glacial Environments in the
1291 Central North Sea Using 3D Seismic and Borehole Data. Ph.D. thesis, University of
1292 London, 410 pp.
1293
1294 Graham, A.G.C., Stoker, M.S., Lonergan, L., Bradwell, T., Stewart, M.A., 2011. The
1295 Pleistocene glaciations of the North Sea Basin. In: Ehlers, J., Gibbard, P.L., Hughes,
1296 P.D. (Eds.), *Quaternary Glaciations – Extent and Chronology – A Closer Look*.
1297 *Developments in Quaternary Sciences*, Elsevier, vol. 15, pp. 261–278.
1298
1299 Gutjahr, M., Hoogakker, B.A.A., Frank, M., McCave, N., 2010. Changes in North
1300 Atlantic Deep Water strength and bottom water masses during Marine Isotope Stage 3
1301 (45-35 ka BP). *Quaternary Science Reviews* 29, 2451-2461.
1302
1303 Hao, Q., Wang, L., Oldfield, F., Guo, Z., 2015. Extra-long interglacial during MIS
1304 15-13 arising from limited extent of Arctic ice sheets in glacial MIS 14. *Scientific*
1305 *Reports* 5, 12103. DOI: 10.1038/srep12103
1306
1307 Hays, J.D., Imbrie, J., Shackleton, N.J., 1976. Variations in the Earth's orbit:
1308 pacemaker of the ice ages. *Science* 194, 1121-1132.
1309

1310 Head, M.J., Gibbard, P.L., 2005. Early-Middle Pleistocene transitions: an overview
1311 and recommendations for the defining boundary. Geological Society, London, Special
1312 Publications 247, 1-18.
1313
1314 Head, M.J., Gibbard, P.L., 2015. Formal subdivision of the Quaternary
1315 System/Period: past, present, and future. Quaternary International 383, 4-35.
1316
1317 Head, M.J., Pillans, B., Farquhar, S.R., 2008. The Early–Middle Pleistocene
1318 Transition: characterization and proposed guide for the defining boundary. Episodes
1319 31, 255-259.
1320
1321 Hein, A.S., Hulton, N.R.J., Dunai, T.J., Schnabel, C., Kaplan, M.R., Naylor, M., Xu,
1322 S., 2009. Middle Pleistocene glaciation in Patagonia dated by cosmogenic-nuclide
1323 measurements on outwash gravels. Earth and Planetary Science Letters 286, 184-197.
1324
1325 Hein, A.S., Cogez, A., Darvill, C.M., Mendelova, M., Kaplan, M.R., Herman, F.,
1326 Dunai, T.J., Norton, K., Xu, S., Christl, M., Rodés, Á. 2017. Regional mid-
1327 Pleistocene glaciation in central Patagonia. Quaternary Science Reviews 164, 77-94.
1328
1329 Hillenbrand, C.-D., Kuhn, G., Frederichs, T., 2009. Record of a Mid-Pleistocene
1330 depositional anomaly in West Antarctic continental sediments: an indicator for ice-
1331 sheet collapse. Quaternary Science Reviews 28, 1147-1159.
1332
1333 Hobbs, W.W., 1945. The Greenland Glacial Anticyclone. Journal of Meteorology 2,
1334 143-153.
1335
1336 Houmark-Nielsen, M., 2004. The Pleistocene of Denmark: a review of stratigraphy and
1337 glaciation history. In: Ehlers, J., Gibbard, P.L. (Eds.), Quaternary Glaciations—
1338 Extent and Chronology. Part I, Europe. Elsevier, Amsterdam, pp. 35–46.
1339
1340 Houmark-Nielsen, M., 2011. Pleistocene glaciations in Denmark: A closer look at
1341 chronology, ice dynamics and landforms. In: Ehlers, J., Gibbard, P.L., Hughes, P.D.
1342 (Eds.), *Quaternary Glaciations – Extent and Chronology – A Closer Look*.
1343 Developments in Quaternary Sciences, Elsevier, vol. 15, pp. 47–58.

1344
1345 Hughes, P.D., Gibbard, P.L., 2018. Global glacier dynamics during 100 ka
1346 Pleistocene glacial cycles. *Quaternary Research* 90, 222-243.
1347
1348 Hughes, P.D., Woodward, J.C., van Calsteren, P.C., Thomas, L.E. 2011. The Glacial
1349 History of The Dinaric Alps, Montenegro. *Quaternary Science Reviews* 30, 3393-
1350 3412.
1351
1352 Hughes, P.D., Gibbard, P.L., Ehlers, J. 2013. Timing of glaciation during the last
1353 glacial cycle: evaluating the meaning and significance of the ‘Last Glacial Maximum’
1354 (LGM). *Earth Science Reviews* 125, 171-198.
1355
1356 Imbrie, J., Hays, J.D., Martinson, D.G., McIntyre, A., Mix, A.C., Morley, J.J., Pisias,
1357 N.G., Prell, W.L., Shackleton, N.J., 1984. The orbital theory of Pleistocene climate:
1358 support from a revised chronology of the marine ¹⁸O record. In: Berger, A., Imbrie, J.,
1359 Hays, G., Kukla, G., Saltzman, B. (Eds.), *Milankovitch and Climate*. Reidel,
1360 Dordrecht, pp. 269–306.
1361
1362 Kiernan, K., Fink, D., Greig, D., Mifud, C., 2010. Cosmogenic radionuclide
1363 chronology of pre-last glacial cycle moraines in the Western Arthur Range, Southwest
1364 Tasmania. *Quaternary Science Reviews* 29, 3286-3297.
1365
1366 Kukla, G., An, Z. S., Melice, J. L., Gavin, J., Xiao, J. L., 1994. Magnetic
1367 susceptibility record of Chinese Loess. *Transactions of the Royal Society of*
1368 *Edinburgh, Earth Science*, **81**, 263–288.
1369
1370 Lambert, F., Delmonte, B., Petit, J.R., Bigler, M., Kaufmann, P.R., Hutterli, M.A.,
1371 Stockler, T.F., Ruth, U., Steffensen, J.P., Maggi, V., 2008. Dust–climate couplings
1372 over the past 800,000 years from the EPICA Dome C ice core. *Nature* 452, 616-619.
1373
1374 Lambert, F., Bigler, M., Steffensen, J.P., Hutterli, M., Fischer, H., 2012. Centennial
1375 mineral dust variability in high-resolution ice core data from Dome C, Antarctica.
1376 *Climate of the Past* 8, 609-623.
1377

1378 Lang, N., Wolff, E.W., 2011. Interglacial and glacial variability from the last 800 ka
1379 in marine, ice and terrestrial archives. *Climate of the Past* 7, 361-380. doi:10.5194/cp-
1380 7-361-2011
1381
1382 Lewis, A.N., 1945. Pleistocene glaciation in Tasmania. *Papers and Proceedings - The*
1383 *Royal Society of Tasmania* 1944, 41-56.
1384
1385 Lindner, L., Marks, L., 1999. New approach to stratigraphy of palaeolake and glacial
1386 sediments of the younger Middle Pleistocene in mid-eastern Poland. *Geological*
1387 *Quarterly* 43 (1), 1-8.
1388
1389 Lisiecki, L.E., Raymo, M.E., 2005. A Pliocene-Pleistocene stack of 57 globally
1390 distributed benthic $\delta^{18}\text{O}$ records. *Paleoceanography* 20, PA1003,
1391 doi:10.1029/2004PA001071
1392
1393 Litt, T., Behre, K.-E., Meyer, K.-D., Stephan, H.-J., and Wansa, S., 2007.
1394 *Stratigraphische Begriffe für das Quartär des norddeutschen Vereisungsgebietes,*
1395 *E&G Quaternary Science Journal* 56, 7-55
1396
1397 Manabe, S., Broccoli, A.J. 1985. The influence of continental ice sheets on the
1398 climate of an ice age. *Journal of Geophysical Research* 90, D1, 2167-2190.
1399
1400 Margari, V., Skinner, L.C., Tzedakis, P.C., Ganopolski, A., Vautravers, M.,
1401 Shackleton, N.J., 2010. The nature of millenniascale climate variability during the
1402 past two glacial periods. *Nature Geoscience* 3, 127-131.
1403
1404 Margari, V., Skinner, L.C., Hodell, D.A., Martrat, B., Toucanne, S., Grimalt, J.O.,
1405 Gibbard, P.L., Lunkka, J.P., Tzedakis, P.C., 2014. Land-ocean changes on orbital and
1406 millennial time scales and the penultimate glaciation. *Geology* 42, 183-186.
1407
1408 Marks, L., 2011. Quaternary glaciations in Poland. In: Ehlers, J., Gibbard, P.L. and
1409 Hughes, P.D. (Eds.), *Quaternary Glaciations – Extent and Chronology: A Closer*
1410 *Look. Developments in Quaternary Science*, 15. Elsevier: Amsterdam, pp. 299-304.
1411

1412 McManus, J.F., Oppo, D.W., Cullen, J.L., 1999. A 0.5 million-year record of
1413 millennial-scale climate variability in the North Atlantic. *Science*, 283, 971-975.
1414

1415 Mercer, J.H., 1984. Simultaneous climatic change in both hemispheres and similar
1416 bipolar interglacial warming: evidence and implications. In: Hansen, J.E., Takahashi,
1417 T., *Climate Processes and Climate Sensitivity*. Geophysical Monograph Series 29,
1418 307-313.
1419

1420 Mudelsee, M., Schulz, M., 1997. The Mid-Pleistocene transition: onset of 100 ka
1421 cycle lags ice volume build-up by 280 ka. *Earth and Planetary Science Letters* 151,
1422 117-123.
1423

1424 Muttoni, G., Carcano, C., Garzanti, E., Ghielmi, M., Piccin, A., Pini, R., et al., 2003.
1425 Onset of Pleistocene glaciations in the Alps. *Geology* 31, 989-992.
1426

1427 Ottesen, D., Dowdeswell, J.A. & Bugge, T. 2014. Morphology, sedimentary infill and
1428 depositional environments of the Early Quaternary North Sea Basin (56-62 Grad N).
1429 *Marine and Petroleum Geology* 56, 123-146.
1430

1431 Pedro, J.B., Jochum, M., Buizert, C., He, F., Barker, S., Rasmussen, S.O., 2018.
1432 Beyond the bipolar seesaw: Towards a process understanding of interhemispheric
1433 cooling. *Quaternary Science Reviews* 192, 27-46.
1434

1435 Peters, J.L., Benetti, S., Dunlop, P., Ó Cofaigh, C., Moreton, S.G., Wheeler, A.J.,
1436 Clark, C.D., 2016. Sedimentology and chronology of the advance and retreat of the
1437 last British-Irish Ice Sheet on the continental shelf west of Ireland. *Quaternary*
1438 *Science Reviews* 140. 101-124.
1439

1440 Pollard, D., DeConto, R.M., 2009. Modelling West Antarctic ice sheet growth and
1441 collapse through the past five million years. *Nature* 458, 329-333.
1442

1443 Preusser, F., Graf, H.R., Keller, O., Krayss, E., Schlüchter, C., 2011. Quaternary
1444 glaciation history of northern Switzerland. *E&G Quaternary Science Journal* 60, 282-
1445 305.

1446
1447 Railsback, L.B., Gibbard, P.L., Head, M.J., Voarintsoa, N.R.G., Toucanne, S., 2015.
1448 An optimized scheme of lettered marine isotope substages for the last 1.0 million
1449 years, and the climatostratigraphic nature of isotope stages and substages. *Quaternary*
1450 *Science Reviews* 111, 94-106.
1451
1452 Rattenbury, M.S., Townsend, D.B., Johnston, M.R., (compilers), 2006. *Geology of*
1453 *the Kaikoura area. Institute of Geological & Nuclear Sciences 1:250,000 Geological*
1454 *Map 13. GNS Science, Lower Hutt, New Zealand.*
1455
1456 Rial, J.A., 1999. Pacemaking the ice ages by frequency modulation of Earth's orbital
1457 eccentricity. *Science* 285, 5427, 564-568.
1458
1459 Richmond, G.M., 1986. Stratigraphy and correlation of glacial deposits of the Rocky
1460 Mountains, the Colorado Plateau & the ranges of the Great Basin. *Quaternary Science*
1461 *Reviews* 5, 99-127.
1462
1463 Richmond, G.M., Fullerton, D.S., 1986. Summation of Quaternary glaciations in the
1464 United States of America. In: Sibrava, V., Bowen, D.Q., Richmond, G.M. (Eds.)
1465 *Quaternary Glaciations in the Northern Hemisphere, Quaternary Science Reviews* 5,
1466 183-196.
1467
1468 Rohling, E. J., Grant, K., Bolshaw, M., Roberts, A. P., Siddall, M., Hemleben, C., and
1469 Kucera, M. 2009. Antarctic temperature and global sea level closely coupled over the
1470 past five glacial cycles. *Nature Geoscience* 2, 500-504.
1471
1472 Rohling, E. J., Grant, K. M., Bolshaw, M., Roberts, A. P., Siddall, M., Hemleben, C.,
1473 Kucera, M., Foster, G. L., Marino, G., Roberts, A. P., Tamisiea, M. E., and Williams,
1474 F., 2014. Sea-level and deep-sea-temperature variability over the past 5.3 million
1475 years. *Nature* 508, 477-482.
1476
1477 Roskosch, J. Winsemann, J., Polom, U., Brandes, C., Tsukamoto, S., Weitkamp, A.,
1478 Bartholomäus, W.A., Henningsen, D., Frechen, M., 2015. Luminescence dating of

1479 ice-marginal deposits in northern Germany: evidence for repeated glaciations during
1480 the Middle Pleistocene (MIS 12 to MIS 6). *Boreas*, 44, 103-126.

1481

1482 Rother, H., Shulmeister, J., Rieser, U., 2010. Stratigraphy, optical dating chronology
1483 (IRSL) and depositional model of pre-LGM glacial deposits in the Hope Valley, New
1484 Zealand. *Quaternary Science Reviews* 29, 576-592.

1485

1486 Roucoux, K.H., Tzedakis, P.C., Frogley, M.R., Lawson, I.T., Preece, R.C., 2008.
1487 Vegetation history of the Marine Isotope Stage 7 interglacial complex at Ioannina,
1488 NW Greece. *Quaternary Science Reviews* 27, 1378-1395.

1489

1490 Roucoux, K.H., Tzedakis, P.C., de Abreu, L., Shackleton, N.J., 2006. Climate and
1491 vegetation changes 180,000 to 345,000 years ago recorded in a deep-sea core off
1492 Portugal. *Earth and Planetary Science Letters* 249, 307-325.

1493

1494 Rovey, C.W., Balco, G., 2011. Summary of early and middle Pleistocene glaciations
1495 in northern Missouri, USA. In: Ehlers, J., Gibbard, P.L., Hughes, P.D. (Eds.),
1496 *Quaternary Glaciations – Extent and Chronology – A Closer Look*. Developments in
1497 Quaternary Sciences, Elsevier, vol. 15, pp. 553-561.

1498

1499 Ruddiman, W.F., McIntyre, A., 1982. Severity and speed of Northern Hemisphere
1500 glaciation pulses: The limiting case? *Geological Society of America Bulletin* 93,
1501 1273-1279.

1502

1503 Ruddiman, W.F., Raymo, M.E., Martinson, D.G., Clement, B.M., Backman, J., 1989.
1504 Pleistocene evolution of Northern Hemisphere climate. *Paleoceanography* 4, 353-412.

1505

1506 Rudenko, T.A., Fainer, Yu.B., Fainer, T.G., 1984. National Geological Map of the
1507 USSR, Scale 1:1 000 000, New Series, Quadrangle P48,49 (Vanavara). Map of
1508 Quaternary Deposits. VSEGEI, Leningrad.

1509

1510 Ruth, U., Bigler, M., Rothlisberger, R., Siggaard-Andersen, M.L., Kipfstuhl, S., Goto-
1511 Azuma, K., Hansson, M.E., Johnsen, S.J., Lu, H.Y., Steffensen, J.P., 2007. Ice core

1512 evidence for a very tight link between North Atlantic and east Asian glacial climate.
1513 Geophysical Research Letters 34 (3), L03706. doi:10.1029/2006GL027876.
1514
1515 Schlüchter, C. 1989. A non-classical summary of the Quaternary stratigraphy in the
1516 northern Alpine Foreland of Switzerland. Bulletin de la Société neuchâteloise de
1517 géographie 32 – 33, 143-157.
1518
1519 Scourse, J.D., Austin, W.E.N., Sejrup, H.P., Ansair, M.H., 1999. Foraminiferal
1520 isoleucine epimerization 353 determinations from the Nar Valley Clay, Norfolk, UK:
1521 implications for Quaternary correlations in the 354 southern North Sea basin.
1522 Geological Magazine 136, 543-560.
1523
1524 Sejrup, H.P., Larsen, E., Landvik, J., King, E.L., Haflidason, H., Nesje, A., 2000.
1525 Quaternary glaciations in southern Fennoscandia: evidence from southwestern
1526 Norway and the northern North Sea region. Quaternary Science Reviews 19, 667-685.
1527
1528 Sejrup, H.P., Hjelstuen, B.O., Dahlgren, K.I.T., Haflidason, H., Kuijpers, A., Nygård,
1529 A., Praeg, D., Stoker, M., Vorren, T.O., 2005. Pleistocene glacial history of the NW
1530 European continental margin. Marine and Petroleum Geology 22, 1111-1129.
1531
1532 Shackleton, N.J., 1967. Oxygen isotope Analyses and Pleistocene Temperatures Re-
1533 assessed. Nature 215, 15-17.
1534
1535 Shakun, J. D., Lea, D.W., Lisiecki, L.E., Raymo, M.E., 2015. An 800-kyr record of
1536 global surface ocean $\delta^{18}\text{O}$ and implications for ice volume-temperature coupling.
1537 Earth and Planetary Science Letters 426, 58-68.
1538
1539 Singer, B., Ackert, R.P., Guillou, H., 2004. $^{40}\text{Ar}/^{39}\text{Ar}$ and K-Ar chronology of
1540 Pleistocene glaciations in Patagonia. Geological Society of America Bulletin 116,
1541 434-450.
1542
1543 Sosdian, S. and Rosenthal, Y., 2009. Deep-Sea Temperature and Ice Volume Changes
1544 Across the Pliocene-Pleistocene Climate Transitions, Science, 325, 306-310.
1545

1546 Spooner, I.S., Osborn, D.G., Barendregt, R.W., Irving, E., 1996. A Middle
1547 Pleistocene (Isotope stage 10) glacial sequence in the Stikine River valley, British
1548 Columbia. *Canadian Journal of Earth Sciences* 33, 1428-1438.
1549
1550 Spratt, R.M., Lisiecki, L.E., 2016. A Late Pleistocene sealevel stack. *Climate of the*
1551 *Past* 12, 1079-1092. doi:10.5194/cp-12-1079-2016
1552
1553 Stoker, M.S., Bradwell, T. 2005. The Minch palaeo-ice stream, NW sector of the
1554 British-Irish ice sheet. *Journal of the Geological Society, London* 162, 425–428.
1555
1556 Stiff, B.J., Hansel, A.K., 2004. Quaternary glaciations in Illinois. In: Ehlers, J.,
1557 Gibbard, P.L. (Eds.), *Quaternary Glaciations—Extent and Chronology*, vol. II, North
1558 America. Elsevier, Amsterdam, pp. 71–82.
1559
1560 Stokes, C., Tarasov, L., Dyke, A.S., 2012. Dynamics of the north American Ice Sheet
1561 Complex during its inception and build-up to the Last Glacial Maximum. *Quaternary*
1562 *Science Reviews* 50, 86-104.
1563
1564 Stocker, T.F., Johnsen, S.J., 2003. A minimum thermodynamic model for the bipolar
1565 seesaw. *Paleoceanography* 18, 4, 1087, doi:10.1029/2003PA00092
1566
1567 Stephan, H-J., 2014. Climato-stratigraphic subdivision of the Pleistocene in
1568 Schleswig-Holstein, Germany and adjoining areas. *E&G Quaternary Science Journal*
1569 63, 3-18.
1570
1571 Sugden, D.E., Bentley, M.J., Ó Cofaigh, C., 2006. Geological and geomorphological
1572 insights into Antarctic ice sheet evolution. *Philosophical Transactions of the Royal*
1573 *Society A* 364, 1607-1625.
1574
1575 Sutter, J., Fischer, H., Grosfeld, K., Karlsson, N.B., Kleiner, T., Van Liefferinge, B.,
1576 Eisen, O., 2019. Modelling the Antarctic Ice Sheet across the mid-Pleistocene
1577 transition – implications for Oldest Ice. *The Cryosphere* 13, 2023-2041.
1578

1579 Svendsen J.I., Alexanderson, H., Astakhov, V.I., Demidov, I., Dowdeswell, J.A.,
1580 Funder, S., Gataullin, V., Henriksen, M., Hjort, C., Houmark-Nielsen, M., Hubberten,
1581 H.-W., Ingólfsson, Ó., Jakobsson, M., Kjær, K.H., Larsen, E., Lokrantz, H., Pekka, J.,
1582 Lunkka Lyså, A., Mangerud, J., Matiouchkov, A., Murray, A., Möller, P., Niessen, F.,
1583 Nikolskaya, O., Polyak, L., Saarnisto, M., Siegert, C., Siegert, M.J., Spielhagen, R.F.,
1584 Stein, R., 2004. Late Quaternary ice sheet history of northern Eurasia. *Quaternary*
1585 *Science Reviews* 23, 1229-1271.

1586
1587

1588 Swanger, K.M., Lamp, J.L., Winckler, G., Schaefer, J.M., Marchant, D.R., 2017.
1589 Glacier advance during Marine Isotope Stage 11 in the McMurdo Dry Valleys of
1590 Antarctica. *Scientific Reports* 7, 41433.

1591

1592 Swingedouw, D., Fichefet, T., Goosse, H., Loutre, M.F., 2009. Impact of transient
1593 freshwater releases in the Southern Ocean in the AMOC and climate. *Climate*
1594 *Dynamics* 33, 365-381.

1595

1596 Syverson, K.M., Colgan, P.M., 2004. The Quaternary of Wisconsin: a review of
1597 stratigraphy and glaciation history. In: Ehlers, J., Gibbard, P.L. (Eds.), *Quaternary*
1598 *Glaciations—Extent and Chronology. Part II: North America*. Elsevier, Amsterdam,
1599 pp. 295–311.

1600

1601 Syverson, K.M., Colgan, P.M., 2011. The Quaternary of Wisconsin: An Updated
1602 Review of Stratigraphy, Glacial History and Landforms. In: Ehlers, J., Gibbard, P.L.,
1603 Hughes, P.D. (Eds.), *Quaternary Glaciations – Extent and Chronology: A Closer*
1604 *Look*. *Developments in Quaternary Science* 15. Elsevier, Amsterdam, p. 537-552.

1605

1606 Tabor, C.R., Poulsen, C.J., 2016. Simulating the mid-Pleistocene transition through
1607 regolith removal. *Earth and Planetary Science Letters* 434, 231-240.

1608

1609 Thierens, M., Pirlet, H., Colin, C., Latruwe, K., Vanhaecke, F., Lee, J.R., Stuut J.-B.,
1610 Titschack, J., Huvenne, V.A.I., Dorschel, B., Wheeler, A.J., Henriot, J.-P. 2012. Ice-
1611 rafting from the British-Irish ice sheet since the earliest Pleistocene (2.6 million years
1612 ago): implications for long-term mid-latitude ice-sheet growth in the North Atlantic
1613 region. *Quaternary Science Reviews* 44, 229-240.

1614

1615 Toucanne, S., Zaragosi, S., Bourillet, J.F., Cremer, M., Eynaud, F., Van Vliet-Lanoe,
1616 B., Penaud, A., Fontanier, C., Turon, J.L., Cortijo, E., Gibbard, P.L., 2009a. Timing of
1617 massive 'Fleuve Manche' discharges over the last 350 kyr: insights into the European
1618 ice-sheet oscillations and the European drainage network from MIS 10 to 2.
1619 *Quaternary Science Reviews* 28, 1238-1256.

1620

1621 Toucanne, S., Zaragosi, S., Gibbard, P.L., Bourillet, J.F., Cremer, M., Eynaud, F.,
1622 Giraudeau, J., Turon, J.L., Cremer, M., Cortijo, E., Martinez, P., Rossignol, L.,
1623 2009b. A 1.2 my record of glaciation and fluvial discharge from the West European
1624 continental margin. *Quaternary Science Reviews* 28, 2974-2981.

1625

1626 Van Husen, D., Reitner, J.M. 2011. An Outline of the Quaternary Stratigraphy of
1627 Austria. *E & G Quaternary Science Journal* 60(2-3), 366-387.

1628

1629 Velichko, A.A., Faustova, M.A., Pisareva, V.V., Gribchenko, Y.N., Sudakova, N.G.,
1630 Lavrentiev, N.V., 2011. Glaciations of the East European Plain—distribution and
1631 chronology. In: Ehlers, J., Gibbard, P.L., Hughes, P.D. (Eds.), *Quaternary*
1632 *Glaciations – Extent and Chronology – A Closer Look*. Developments in Quaternary
1633 Sciences, Elsevier, vol. 15, pp. 337-360.

1634

1635 Vidal Romani, Fernández, Mosquera, D., Marti, K., 2015. The glaciation of Serra de
1636 Quiexa-Invernadoiro and Serra do Gerês, NW Iberia. A critical review and a
1637 cosmogenic nuclide (^{10}Be and ^{21}Ne) chronology. *Cadernos Laboratorio Xeolóxico de*
1638 *Laxe*, 38, 27-45.

1639

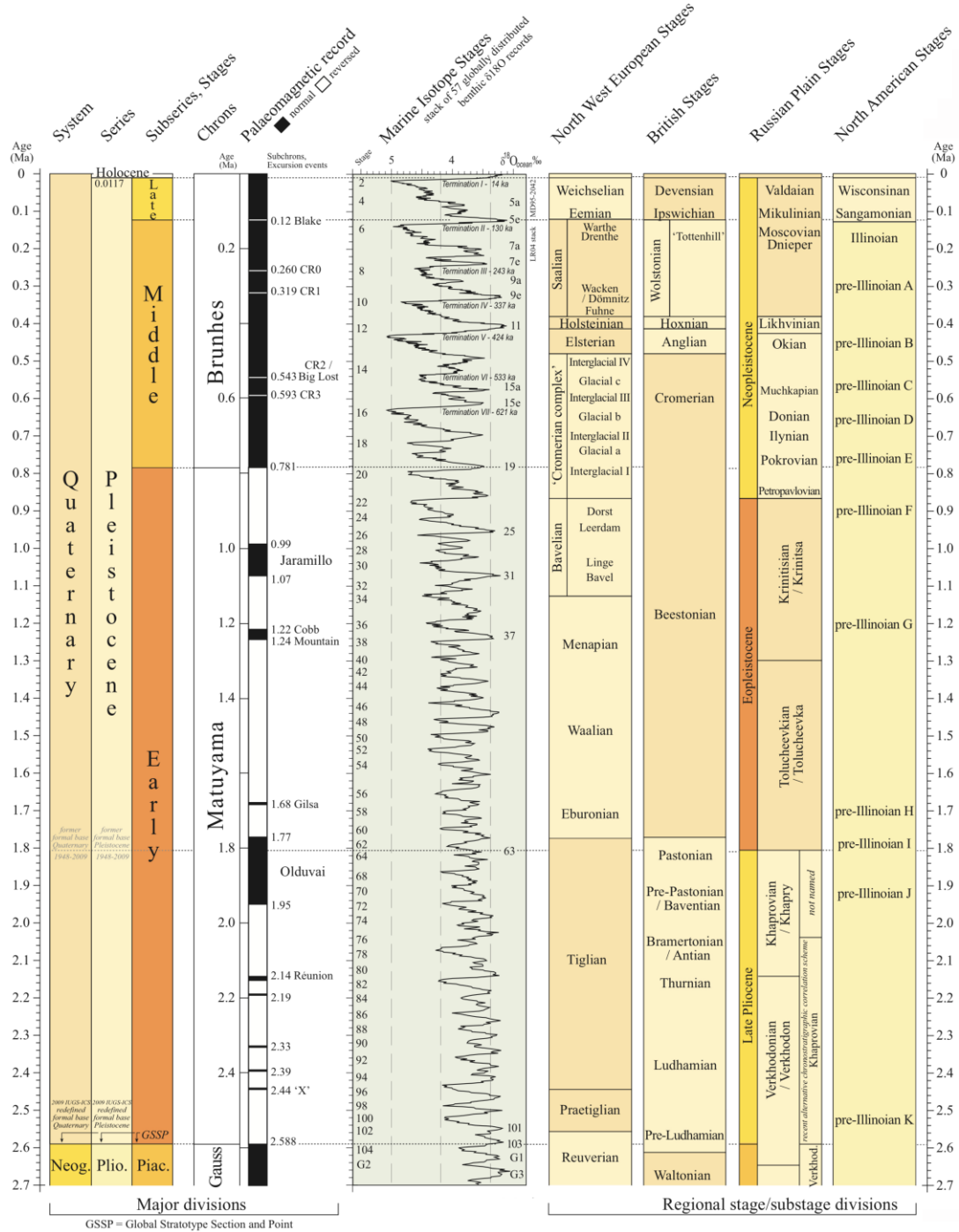
1640 Waelbroeck, C., Labeyrie, L., Michel, E., Duplessy, J.C., McManus, J.F., Lambeck,
1641 K., Balbon, E., Labracherie, M., 2002. Sea-level and deep water temperature changes
1642 derived from benthic foraminifera isotopic records. *Quaternary Science Reviews* 21,

1643 295-305.
1644
1645
1646 Ward, B.C., Bond, J.D., Froese, D., Jensen, B., 2008. Old Crow tephra (14010 ka)
1647 constrains penultimate Reid glaciation in central Yukon Territory. *Quaternary Science*
1648 *Reviews* 27, 1909-1915.
1649
1650 White, T.S., Bridgland, D.R., Howard, A.J., Westaway, R., White, M.J., 2010.
1651 Evidence from the Trent terrace archive, Lincolnshire, UK, for lowland glaciation of
1652 Britain during the Middle and Late Pleistocene. *Proceedings of the Geologists'*
1653 *Association* 121, 141-153.
1654
1655 White, T.S., Bridgland, D.R., Westaway, R., Straw, A., 2017. Evidence for a late
1656 Middle Pleistocene glaciation of the British margin of the southern North Sea. *Journal*
1657 *of Quaternary Science* 32, 261-275.
1658
1659 Willeit, M., Ganopolski, A., Calov, R., Brovkin, V., 2019. Mid-Pleistocene transition
1660 in glacial cycles explained by declining CO₂ and regolith removal. *Science Advances*
1661 5, eaav7337. 8 pp.
1662

1663 **Figures**

1664

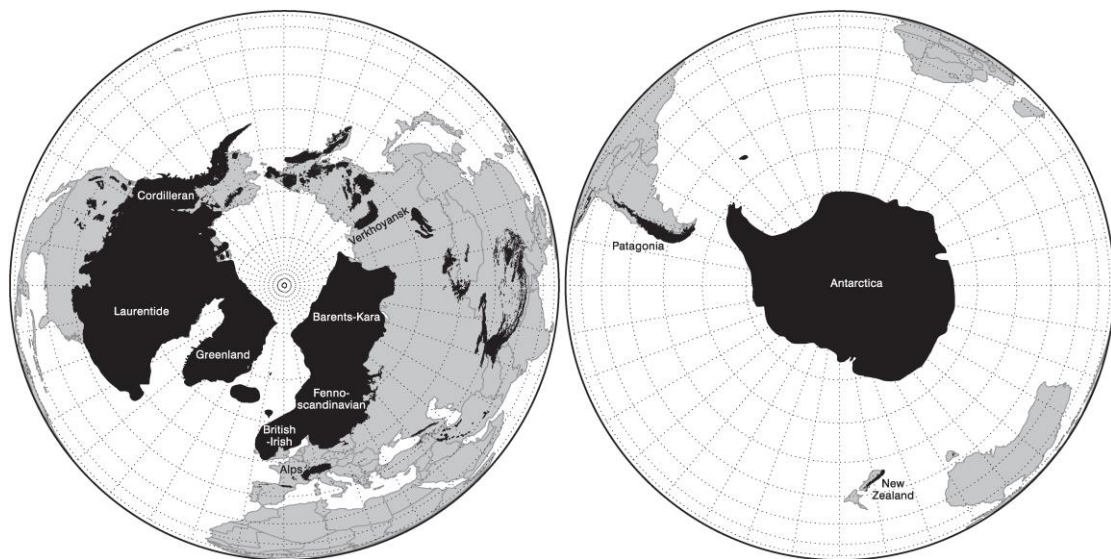
1665 **Figure 1.** Global correlations between terrestrial glacial chronostratigraphical terms
1666 and the marine oxygen isotope record. Adapted from the global chronostratigraphical
1667 correlation table for the past 2.7 million years by Cohen and Gibbard (2011).



1668

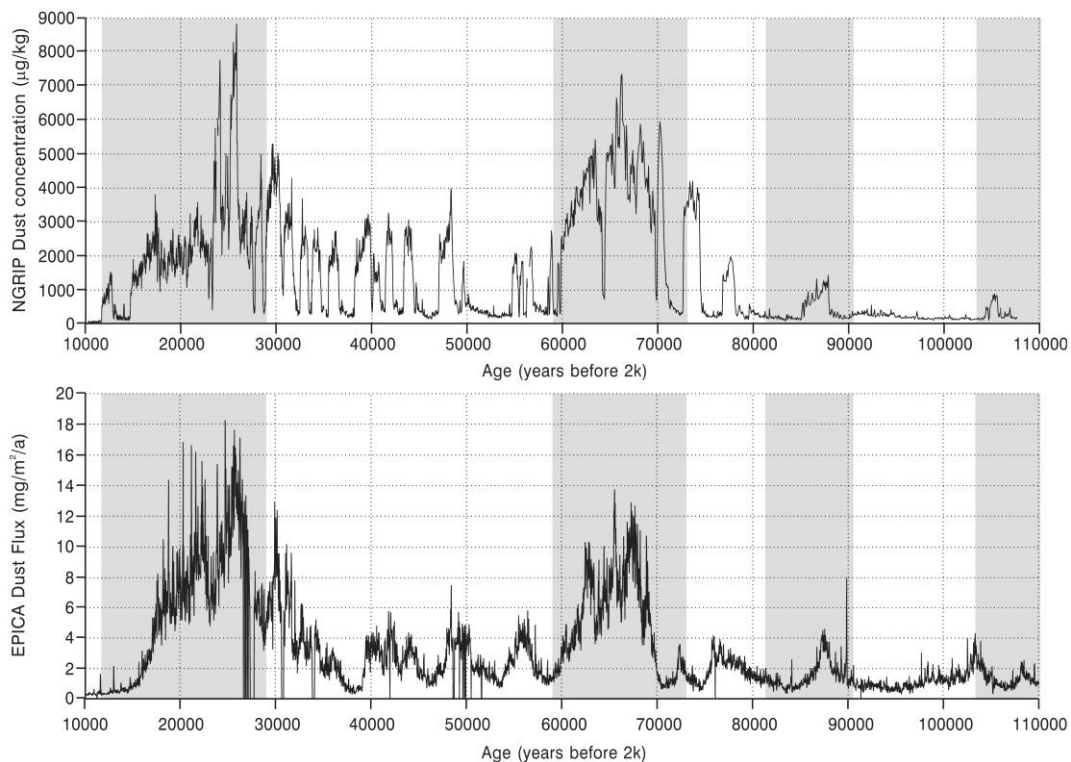
1669

1670 **Figure 2.** Maximum extent of glaciation around the globe during the last glacial-
1671 interglacial cycle (Weichselian, Wisconsinan, Valdaian Stage and equivalents). The
1672 extents depicted here are diachronous with ice masses reaching their maximum
1673 positions at different times. The extents would have also varied in different glacial-
1674 interglacial cycles, although the general differences in extents of the largest
1675 continental ice masses is typical of the relative contributions of ice on Earth by the
1676 major regional ice masses. This figure illustrates the relative sizes of the ice masses
1677 and their spatial distributions and highlights the spatial dominance of the ice masses
1678 in the Northern Hemisphere. Redrawn and adapted from Ehlers and Gibbard (2007)
1679 and Hughes et al. (2013).



1680
1681
1682
1683

1684 **Figure 3.** The dust records from Greenland (NGRIP) and Antarctica (EPICA) ice
1685 cores for the last glaciation in MIS 5d-2. The top diagram shows the dust
1686 concentration (Ruth et al., 2007) record from the NGRIP core (on the GICC05 age
1687 model). The bottom diagram shows dust flux (Lambert et al., 2012) from EPICA,
1688 Antarctica (on the EDC3 age model). The records show a strong correlation in dust
1689 records between Greenland and Antarctica and this supports the assertion that dust
1690 records in either polar hemisphere reflect the state of the global hydrological cycle
1691 and the global atmosphere. This observation provides the template for interpreting
1692 earlier glaciations with drier and dustier atmosphere directly related to increasing
1693 global ice coverage. This interhemispheric comparability is important because
1694 beyond the last interglacial reliance has currently to be made on the Antarctic ice-core
1695 records.

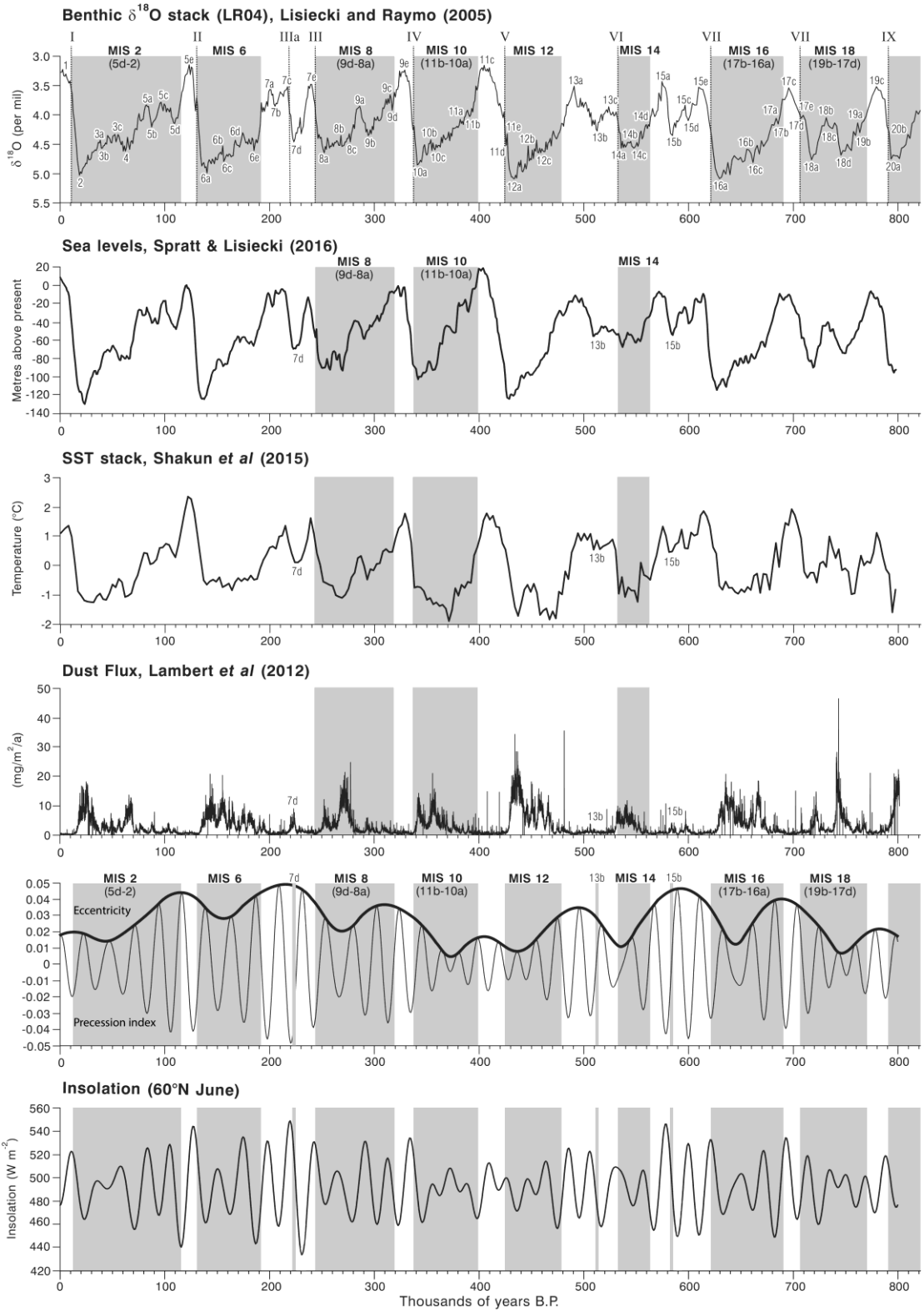


1696
1697
1698

1699 **Figure 4.** Graphs showing link between the structure of glacial-interglacial cycles
1700 indicated in the global benthic stack of Lisiecki and Raymo (2005), global sea levels
1701 extracted from a global of seven sea-level records (from Spratt and Lisiecki 2016),
1702 global sea-surface temperatures from a 49 paired sea-surface temperature-planktonic
1703 $\delta^{18}\text{O}$ records (Shakun et al. 2015) and dust flux from the EPICA Dome C ice-core
1704 record (Lambert et al. 2012). The Roman numerals (I, II, III, IV etc.) over the global
1705 benthic stack indicate the positions of the respective glacial terminations. The lower
1706 two graphs illustrate solar parameters for the last 800 ka. The second from bottom
1707 graph shows the precession index and the eccentricity index from Berger and Loutre
1708 (1991) and Berger (1992). The precession index (climatological precession parameter:
1709 $e \sin \omega$; values from -1 to +1) is an indicator of the amplitude of the seasonal cycle
1710 with a move towards autumn/winter perihelion at peaks and towards an earlier
1711 spring/summer perihelion at troughs and is determined by the variations in
1712 eccentricity (dimensionless value between 0 and 1). The bottom graph shows June
1713 insolation data at 60°N (Berger and Loutre 1991; Berger 1992).

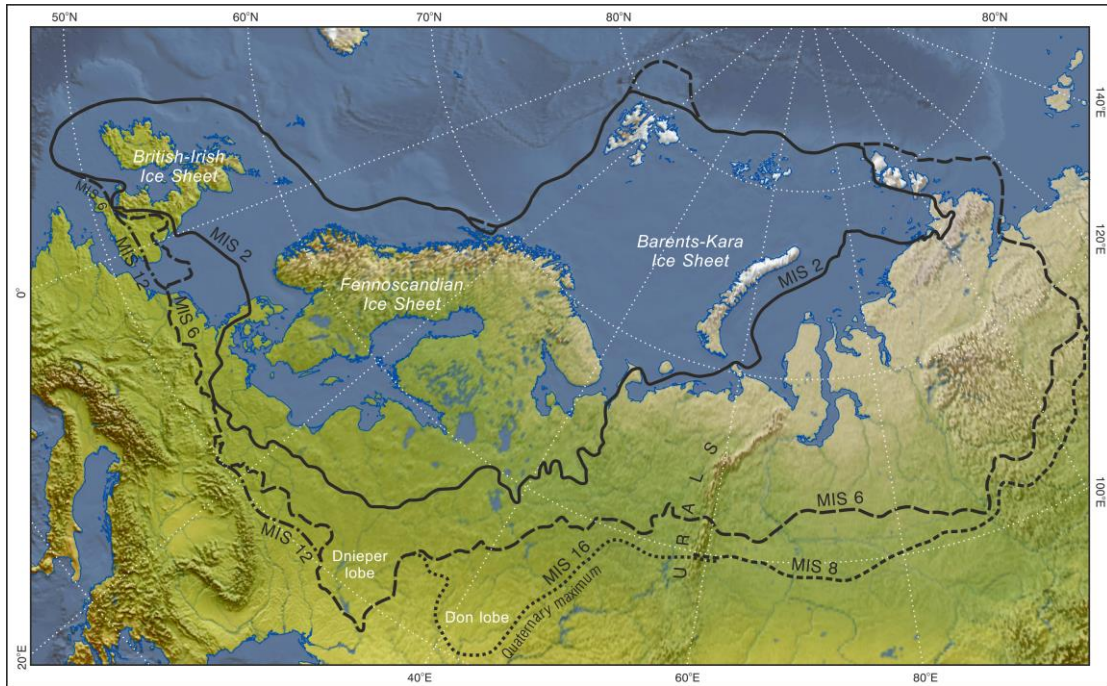
1714
1715

See next page



1716
1717
1718

1719 **Figure 5.** Limits of the Eurasian contiguous ice sheets during the Middle and Late
1720 Pleistocene. Adapted from information in Svendsen et al. (2004), Ehlers and Gibbard
1721 (2004), and Astakhov et al. (2016). East of the Urals, the most extensive glaciation
1722 occurred in MIS 8, although evidence of this glaciation is largely absent to the west in
1723 Europe.



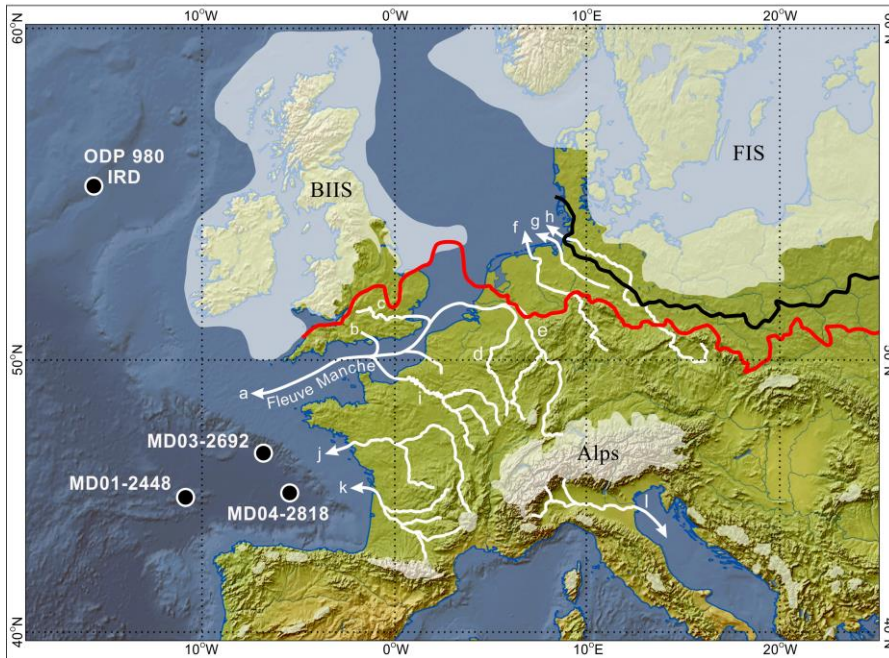
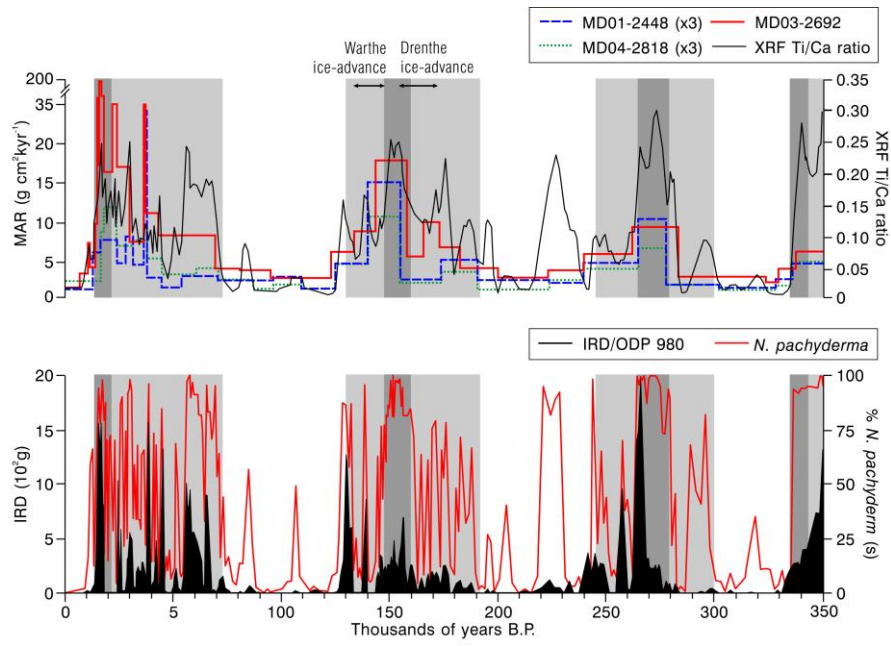
1724
1725

1726 **Figure 6.** Top diagram: mass accumulation rates (MAR) in marine sediment records
1727 in the Bay of Biscay, NE Atlantic Ocean (from Toucanne et al. 2009a). The MAR
1728 graph is from sites MD03-2692 (46°49.720'N, 9°30.970'W), MD01-2448 and MD04-
1729 2818. Lower mass accumulation rates (MAR) in MIS 10 and 8 compared with MIS
1730 5d-2 and 6 are interpreted as indicating less glaciofluvial discharge, primarily through
1731 the former English Channel fluvial system (Fleuve Manche). The XRF Ti-Ca ratio
1732 reflects terrigenous sediment input, but is also associated with an ice-rafted debris
1733 source. The ice-rafted debris (IRD) graph is from site ODP 980 from further north in
1734 the NE Atlantic Ocean (55°29'N, 14°42'W) off the British-Irish continental shelf
1735 (data from McManus et al. 1999). The bottom map shows the locations of these core
1736 sites relative to the former ice masses. The approximate positions of the Late
1737 Pleistocene ice limits for the northern ice sheets (BIIS = British-Irish Ice Sheet; FIS=
1738 Fennoscandian Ice Sheet) are given for reference in white shading together with the
1739 Late Saalian (MIS 6) ice limits shown in red/grey [Drenthe advance] and black
1740 [Warthe advance]. The outlines and positions of ice masses in central and southern
1741 Europe are schematic due to scale. The white arrows and the associated lowercase
1742 letters identify the main European rivers: a: 'Fleuve Manche', b: Solent, c: Thames, d:
1743 Meuse, e: Rhine, f: Ems, g: Wesser, h: Elbe, i: Seine, j: Loire, k: Gironde, l: Pô.
1744 Redrawn and adapted from Toucanne et al. (2009a).

1745

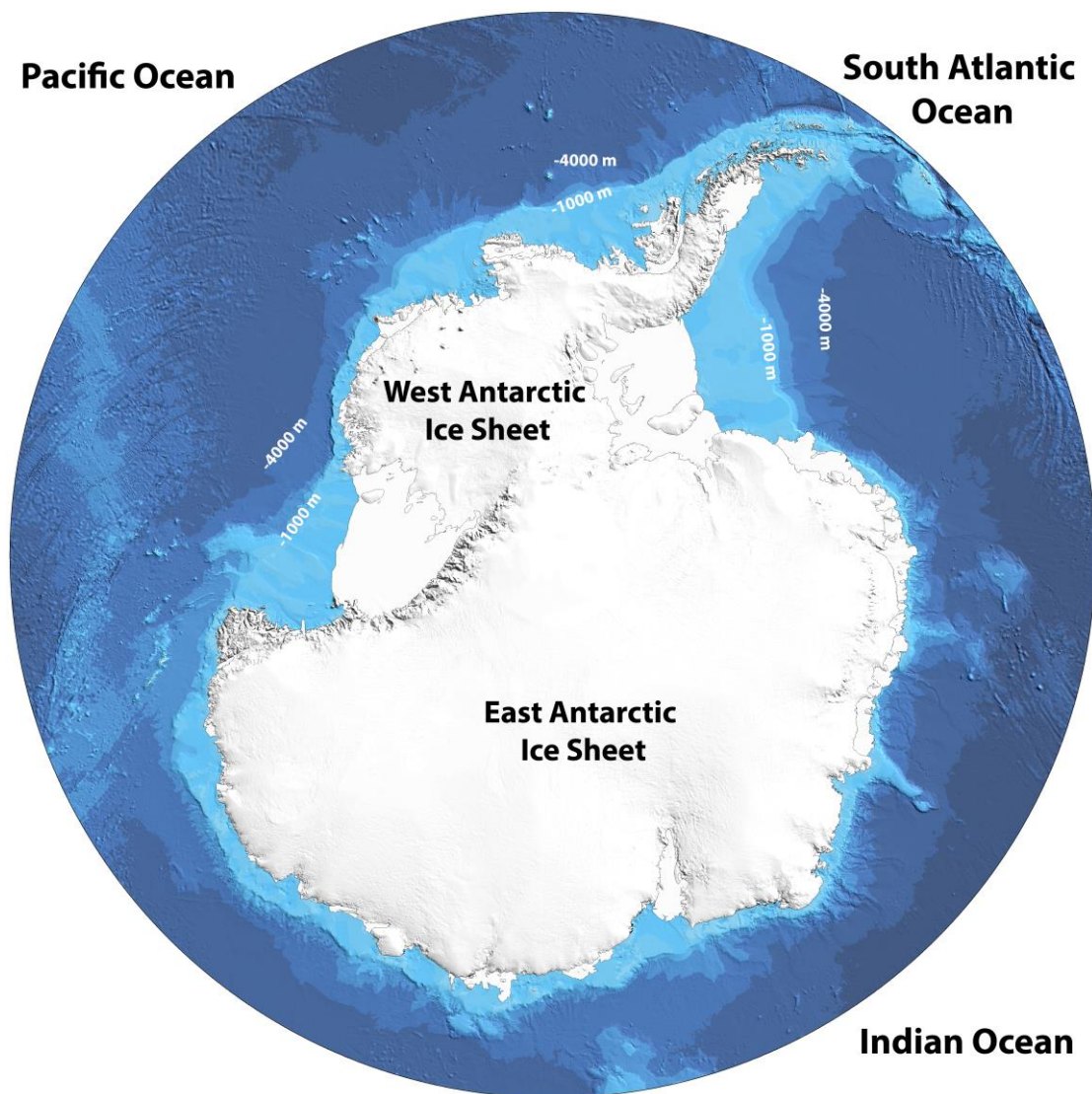
1746

See next page



1747
1748

1749 **Figure 7.** Topographic map of Antarctica showing offshore bathymetry. The largest
1750 area of the currently unglaciated continental shelf is off West Antarctica. This means
1751 that there was likely to have been greater scope for ice-sheet expansion to the shelf
1752 edge during Pleistocene glaciations than around the East Antarctic Ice Sheet. Thus,
1753 the West Antarctic Ice Sheet would have been the most significant ice mass in the
1754 Southern Hemisphere in terms of changing dynamics through glacial-interglacial
1755 cycles. From the International Bathymetric Chart of the Southern Ocean (IBCSO)
1756 Version 1.0 (Arndt et al. 2018). <https://www.scar.org/science/ibcsso/resources/>
1757



1758
1759
1760
1761
1762

1763 **Tables**

1764

1765 **Table 1.** Sea-level estimates from the global stack of Spratt and Lisiecki (2016) in
 1766 order of magnitude. These values are obtained from the long stack (0-798 ka) of five
 1767 sea level reconstructions. The marine isotope stages listed represent cold-climate
 1768 intervals within glacial-interglacial cycles. *MIS 15b, 13b and 7d are stadials within
 1769 interglacials (cf. Hughes et al. 2018).

	MIS	Global sea-level minima (m) – in descending order of magnitude
	2	-130
	6	-124.5
	12	-124.4
	16	-114.62
“Missing glaciations”	10	-102.83
	8	-93.27
	7d*	-68.74
	14	-67.39
	13b*	-55.45
	15b*	-54.40

1770

1771

1772 **Table 2.** Solar radiation peak-trough amplitude at 60°N early in cold stages or at the end of preceding interglacials. Solar-trough magnitude
 1773 describes the peak-trough magnitude and timespan. This is derived by taking the median value between the preceding solar peak and subsequent
 1774 trough and scaling (dividing) this by the peak to trough timespan, then inverting this calculated value. Solar radiation data are derived from
 1775 Berger and Loutre (1991) and Berger (1992).

	Marine Isotope Stage	preceding peak*	age (ka)	trough*	age (ka)	amplitude change	median peak-trough*	peak-trough timespan (kyr)	solar-trough magnitude
	MIS 7/6	531.96	198	443.00	187	88.96	487.48	<i>11</i>	<i>0.0226</i>
	MIS 13/12	525.83	486	456.22	475	69.61	491.03	<i>11</i>	<i>0.0224</i>
	MIS 17/16	534.77	693	448.99	682	85.78	491.88	<i>11</i>	<i>0.0224</i>
	MIS 5e/5d-2	544.69	127	440.20	116	104.49	492.45	<i>11</i>	<i>0.0223</i>
“Missing glaciations”	MIS 9/8	517.25	313	459.83	303	57.42	488.54	<i>10</i>	<i>0.0205</i>
	MIS 11/10	508.45	373	484.84	363	23.61	496.65	<i>10</i>	<i>0.0201</i>
	MIS 15/14	546.62	579	454.66	567	91.96	500.64	<i>12</i>	<i>0.0240</i>

1776

1777 * insolation (W m^{-2})

1778